Washington University School of Medicine
Digital Commons@Becker

Open Access Publications

2021

Mechanical dysfunction of the sarcomere induced by a pathogenic mutation in troponin T drives cellular adaptation

Sarah R. Clippinger

Paige E. Cloonan

Wei Wang

Lina Greenberg

W. Tom Stump

See next page for additional authors

Follow this and additional works at: https://digitalcommons.wustl.edu/open_access_pubs

Authors

Sarah R. Clippinger, Paige E. Cloonan, Wei Wang, Lina Greenberg, W. Tom Stump, Paweorn Angsutararux, Jeanne M. Nerbonne, and Michael J. Greenberg

JGP Journal of General Physiology

ARTICLE

Mechanical dysfunction of the sarcomere induced by a pathogenic mutation in troponin T drives cellular adaptation

Sarah R. Clippinger[1], Paige E. Cloonan[1], Wei Wang[2], Lina Greenberg[1], W. Tom Stump[1], Paweorn Angsutararux[3], Jeanne M. Nerbonne[2], and Michael J. Greenberg[1]

Familial hypertrophic cardiomyopathy (HCM), a leading cause of sudden cardiac death, is primarily caused by mutations in sarcomeric proteins. The pathogenesis of HCM is complex, with functional changes that span scales, from molecules to tissues. This makes it challenging to deconvolve the biophysical molecular defect that drives the disease pathogenesis from downstream changes in cellular function. In this study, we examine an HCM mutation in troponin T, R92Q, for which several models explaining its effects in disease have been put forward. We demonstrate that the primary molecular insult driving disease pathogenesis is mutation-induced alterations in tropomyosin positioning, which causes increased molecular and cellular force generation during calcium-based activation. Computational modeling shows that the increased cellular force is consistent with the molecular mechanism. These changes in cellular contractility cause downstream alterations in gene expression, calcium handling, and electrophysiology. Taken together, our results demonstrate that molecularly driven changes in mechanical tension drive the early disease pathogenesis of familial HCM, leading to activation of adaptive mechanobiological signaling pathways.

Introduction

Hypertrophic cardiomyopathy (HCM) is the leading cause of sudden cardiac death in people younger than 30 yr. HCM is characterized by hypertrophy of the left ventricular wall and interventricular septum, myocyte disarray, fibrosis, and diastolic dysfunction. HCM is also associated with marked alterations in cardiomyocyte function, including changes in electrophysiology, contractility, and calcium handling (Harvey and Leinwand, 2011). Large-scale sequencing of families has revealed that HCM is caused by mutations in sarcomeric proteins involved in cardiac contraction, including troponin T (Watkins et al., 1995).

The disease presentation in HCM is quite complex, with functional differences seen at scales ranging from molecules to tissues; however, the molecular triggers that drive the disease pathogenesis are alterations in the abundance, stability, and/or functionality of mutant protein (Greenberg and Tardiff, 2021). This initial trigger activates downstream adaptive and maladaptive processes, some of which can take years to decades to manifest, including ventricular remodeling, and eventually symptomatic disease. Given the inherent complexity of HCM, it has been challenging to link the molecular and cellular phenotypes and to dissect the initial biophysical trigger from secondary adaptive processes.

To better understand the initial molecular insult and its connection to cellular dysfunction in early HCM disease pathogenesis, we examined a pathogenic mutation in troponin T, R92Q (Fig. 1 A), identified in several unrelated families, that causes pronounced ventricular hypertrophy and a relatively high incidence of sudden cardiac death (Watkins et al., 1995). R92Q has been studied in model systems, including feline (Marian et al., 1997) and rat (Rust et al., 1999) cardiomyocytes, rabbit skeletal myofibrils (Morimoto et al., 1998), quail myotubes (Sweeney et al., 1998), and transgenic mice (Tardiff et al., 1999). These studies have reached conflicting conclusions about the effects of the mutation, in part due to phenotypic differences between species. For example, the widely studied transgenic mouse model of R92Q (Tardiff et al., 1999) recapitulates some, but not all, aspects of the human disease phenotype. Elegant

[1]Department of Biochemistry and Molecular Biophysics, Washington University School of Medicine, St. Louis, MO; [2]Cardiovascular Division, Department of Medicine, Washington University School of Medicine, St. Louis, MO; [3]Department of Biomedical Engineering, Washington University, St. Louis, MO.

Correspondence to Michael J. Greenberg: greenberg@wustl.edu

A preprint of this paper was posted at *bioRxiv* on May 5, 2020.

© 2021 Clippinger et al. This article is distributed under the terms of an Attribution–Noncommercial–Share Alike–No Mirror Sites license for the first six months after the publication date (see http://www.rupress.org/terms/). After six months it is available under a Creative Commons License (Attribution–Noncommercial–Share Alike 4.0 International license, as described at https://creativecommons.org/licenses/by-nc-sa/4.0/).

Check for updates

Downloaded from http://rupress.org/jgp/article-pdf/153/5/e202012787/1413510/jgp_202012787.pdf by Washington University In St. Louis Libraries user on 01 May 2021

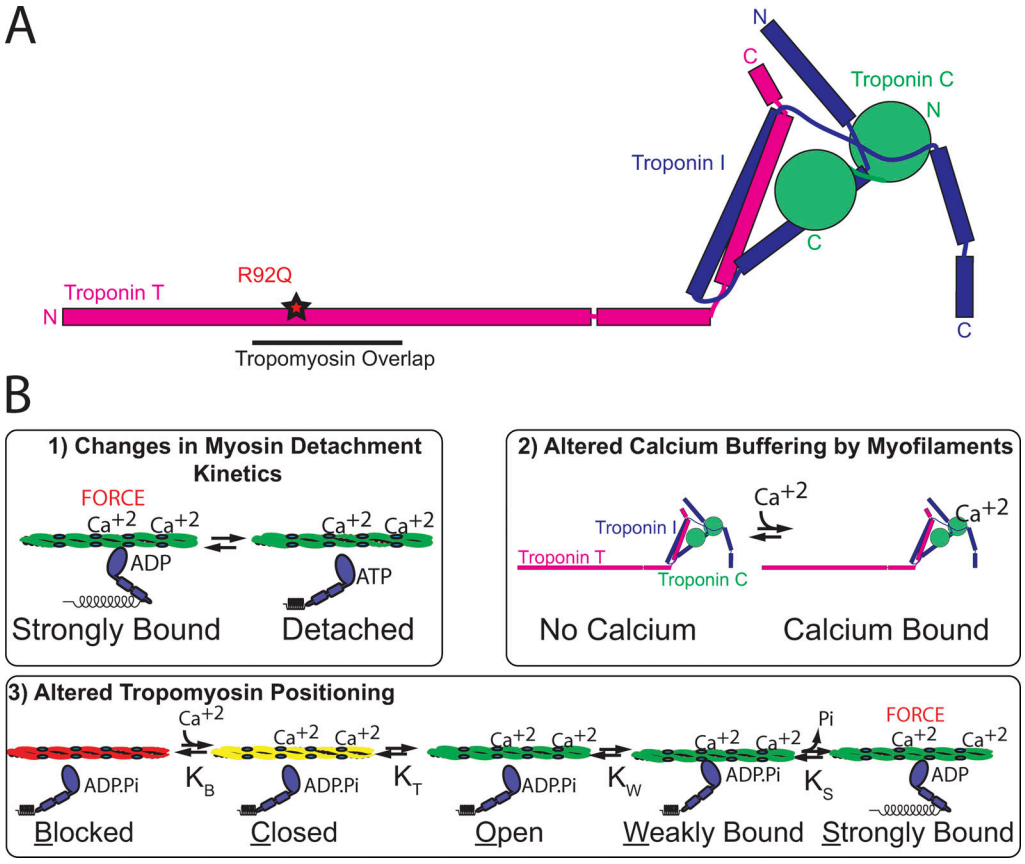

Figure 1. **R92Q mutation in troponin T causes HCM. (A)** Cartoon of the troponin complex (based on Sheng and Jin, 2014). R92Q is located in the region of troponin T that interacts with tropomyosin, near the tropomyosin overlap region. **(B)** Models for the molecular mechanism of R92Q.

experiments by the Tardiff laboratory showed that the disease presentation in mice depends on the myosin heavy chain isoform expressed, with different phenotypes seen when using the faster (*MYH6*) isoform found in mouse ventricles or the slower (*MYH7*) isoform found in human ventricles (Ford et al., 2012). This highlights the need to study the mutation in humanized systems.

Troponin T is part of the troponin complex, which, together with tropomyosin, regulates the calcium-dependent interactions between myosin and the thin filament that power muscle contraction. Biochemical (McKillop and Geeves, 1993) and structural (Lehman et al., 1994) measurements demonstrated that tropomyosin can lie in three states along the thin filament (Fig. 1 B). In the absence of calcium, tropomyosin lies in the blocked position and inhibits the binding of force-generating actomyosin cross-bridges. When calcium binds to troponin C, tropomyosin shifts to the closed position. The tropomyosin can then be pushed into the open position by either thermal fluctuations or myosin weak binding. Once weakly associated with the thin filament, myosin isomerizes into the strong binding state, generating force. The amount of force developed will be proportional to the number of strongly bound, force-generating myosin cross-bridges.

Three models have been put forward to describe the initial molecular insult that drives the R92Q disease pathogenesis (Fig. 1 B): (1) R92Q could affect the cycling kinetics of myosins bound to the thin filament (Ford et al., 2012); (2) R92Q could increase the calcium affinity of troponin, leading to altered calcium buffering by myofilaments that directly disrupts calcium homeostasis (Schober et al., 2012; Ferrantini et al., 2017; Robinson et al., 2018); or (3) R92Q could alter the distribution of positions assumed by tropomyosin along the thin filament, changing the number of bound myosin cross-bridges (McConnell et al., 2017). The mechanistic differences among these models have important implications for the design of therapeutic strategies.

Here, we set out to identify the initial molecular insult in troponin T caused by the R92Q mutation and link the molecular defect to observed derangements in cellular function. To do this, we developed a human R92Q model in gene-edited human induced pluripotent stem cell–derived cardiomyocytes (hiPSC-CMs). We show that the initial biophysical insult is altered positioning of tropomyosin along the thin filament, which directly affects cellular tension, leading to secondary adaptive changes in calcium homeostasis, gene expression, and electrophysiology. Our results implicate mechanobiological signaling as a primary driver of HCM disease pathogenesis.

Materials and methods

Protein modification and purification

Cardiac myosin and actin were purified from cryoground porcine ventricles (Pelfreez) as previously described (Clippinger

Downloaded from http://rupress.org/jgp/article-pdf/153/5/e202012787/1413510/jgp_202012787.pdf by Washington University In St. Louis Libraries user on 01 May 2021

et al., 2019). S1 myosin was prepared by chymotrypsin digestion as previously described (Clippinger et al., 2019). Recombinant human cardiac tropomyosin, troponin I, troponin T, and troponin C were expressed in *Escherichia coli* and purified from BL21-CodonPlus cells (Agilent) as described previously (Clippinger et al., 2019). Purified tropomyosin was reduced in 50 mM dithiothreitol (DTT) at 56°C for 5 min and ultracentrifuged to remove aggregates immediately before being used in each assay. The R92Q mutation was introduced into troponin T using QuickChange Site-Directed Mutagenesis (Agilent), and the presence of the mutation was verified by sequencing.

For the studies of calcium binding, we used IAANS (6-((4-((2-iodoacetyl)amino)phenyl)amino)-2-naphthalenesulfonic acid)–labeled troponin C (Davis et al., 2007). IAANS was custom synthesized by Toronto Research Chemicals. Troponin C^{T53C} was labeled with fivefold molar excess IAANS dye overnight, and the reaction was quenched with DTT. Excess dye was dialyzed out with four dialysis buffer changes of 1 mM DTT, 0.01% NaN_3, 50 µM $CaCl_2$, 1 mM $MgCl_2$, 3 M urea, 1 M KCl, 5 mg/liter tosyl phenylalanyl chloromethyl ketone (TPCK), 5 mg/liter tosyl-L-lysyl-chloromethane hydrochloride (TLCK), and 0.3 mM PMSF (Davis et al., 2007). The IAANS-labeled troponin C^{T53C} was then purified over a MonoQ column and complexed with troponins T and I as done previously (Clippinger et al., 2019).

In vitro motility assays

In vitro motility assays were conducted using thin filaments containing R92Q troponin T as previously described (Clippinger et al., 2019). Data for WT troponin T are from Clippinger et al. (2019). Briefly, enzymatically inactive full-length porcine cardiac myosin was removed by cosedimentation with phalloidin-stabilized F-actin in the presence of ATP. Flow cells were loaded with 1 vol (50 µl) 200 nM myosin, 2 vol 1 mg/ml BSA, 1 vol 1 µM F-actin, 2 vol KMg25 (25 mM KCl, 4 mM $MgCl_2$, 1 mM EGTA, 1 mM DTT, and 60 mM MOPS, pH 7.0) + 1 mM MgATP, 4 vol KMg25, and 1 vol 40 nM rhodamine-phalloidin–labeled thin filaments. After loading 2 vol activation buffer (KMg25 with 4 mM MgATP, 1 mg/ml glucose, 192 U/ml glucose oxidase, 48 µg/ml catalase, 2 µM troponin and tropomyosin, and 0.5% methyl cellulose), flow cells were imaged for 20 frames. Each buffer was balanced to give the desired free calcium, free magnesium, and ionic strength using MaxChelator (Bers et al., 2010). Individual motile filaments were manually tracked using the MTrackJ plugin in Fiji ImageJ (Schindelin et al., 2012), and each point shows the average and standard deviation of the speed from three separate experiments.

Stopped-flow transient kinetic measurement of K_B and ADP release

An SX-20 stopped-flow apparatus (Applied Photophysics) was used. K_B, the equilibrium constant between the blocked and closed states, was determined as previously described (Barrick et al., 2019; Clippinger et al., 2019). WT data are from Clippinger et al. (2019). At both low (pCa 9) and high calcium (pCa 4), 5 µM phalloidin-stabilized pyrene actin, 2 µM tropomyosin, 2 µM troponin, and 0.04 U/ml apyrase were rapidly mixed with 0.5 µM S1 myosin and 0.04 U/ml apyrase. Performed at 20°C, each experiment was the average of at least three separate mixes, and the data were fit by a single exponential curve. K_B was calculated from

$$\frac{k_{obs}(-Ca^{2+})}{k_{obs}(+Ca^{2+})} = \frac{K_B}{1+K_B}. \quad (1)$$

The reported K_B is the average of at least three different experiments. The P value was calculated from a two-tailed Student's *t* test.

The rate of ADP release from myosin bound to regulated thin filaments (20°C) was measured as previously described. (Clippinger et al., 2019) The average and standard deviation of the rate of at least four experiments was calculated and the P value was derived using a two-tailed Student's *t* test.

Fluorescence titrations to measure K_W, K_T, and n

A SX-20 stopped-flow fluorometer was used for all fluorescence titrations. The values of K_W (the equilibrium constant for myosin weak binding), K_T (the equilibrium constant between the closed and open states), and n (the cooperativity) were determined for R92Q and WT using fluorescence titrations as previously described (Barrick et al., 2019; Clippinger et al., 2019). The WT data are from Clippinger et al. (2019). Hypothesis testing and uncertainty estimation were done using established techniques (Efron, 1979; Press, 1992; Martin, 2007). Briefly, the data were resampled using a bootstrapping algorithm, resampled data were fit to calculate 95% confidence intervals, and P values were calculated from the overlap regions between the distributions of bootstraps (Efron, 1979; Press, 1992; Martin, 2007; Barrick et al., 2019).

Measurement of calcium binding to troponin C

The calcium affinity for the troponin complex (Tn^{IAANS}) was determined by titrating regulated thin filaments with increasing calcium concentrations and measuring the change in fluorescence in IAANS-labeled troponin C upon calcium binding (Davis et al., 2007). Tn^{IAANS} was excited at 330 nm and fluorescence emission was detected using a 395 nm long-pass filter. 0.15 µM Tn^{IAANS} complex, 0.45 µM tropomyosin, and 2 µM actin were mixed with increasing concentrations of calcium in 10 mM MOPS, pH 7.0, 150 mM KCl, 3 mM $MgCl_2$, and 1 mM DTT. Each buffer was balanced to give the desired free calcium, free magnesium, and ionic strengths using MaxChelator (Bers et al., 2010). The solution was allowed to equilibrate for 1 min after mixing with constant stirring before the fluorescence intensity was measured. The titration curve was fit by the logistic sigmoid function, which is mathematically equivalent to the Hill equation:

$$Y = Y_{min} + \frac{Y_{max} - Y_{min}}{1 + \exp[(-H(X - pCa_{50})]}, \quad (2)$$

where Y_{max} and Y_{min} are the maximum and minimum IAANS fluorescence, X is the negative logarithm of $[Ca^{2+}]_{free}$, pCa_{50} is the negative log of the concentration of free calcium producing half-maximal fluorescence, and H is the cooperativity (proportional to the Hill coefficient; Tikunova et al., 2002). Titrations

Downloaded from http://rupress.org/jgp/article-pdf/153/5/e202012787/1413510/jgp_202012787.pdf by Washington University In St. Louis Libraries user on 01 May 2021

were performed at both 15°C and 20°C to facilitate comparison with previous measurements using different proteins (Liu et al., 2012). For the measurements at 37°C (Fig. S1), we used a Horiba fluorometer. We excited the fluorophore at 330 nm and integrated the fluorescence >500 nm (Davis et al., 2007). Data were analyzed with the same methodology.

Computational modeling of sarcomeric contractility

To simulate the effects of the experimentally determined changes in equilibrium constants on force production, we used the computational model developed by Campbell et al. (2010), based on McKillop and Geeves (1993), as we have done previously (Clippinger et al., 2019). Briefly, in this model, nine sarcomeres are simulated, where the equilibrium constants between states and a coupling constant describing cooperativity define the probability of switching between biochemical states. The steady-state force is calculated from the equilibrium distribution of states at a given calcium concentration. Our biochemical experiments demonstrated that the primary change at the molecular scale with the mutation is an increase in K_B, such that K_B (R92Q) = 2.56 × K_B (WT). To simulate the WT, we used the default model parameters. To simulate the mutant, we decreased the reverse rate constant that defines K_B, so that K_B (R92Q) = 2.56 × K_B (WT). To simulate the force per sarcomere in response to a calcium transient for the WT, we used the default calcium transient. To simulate the response of R92Q, we changed K_B as described above and we reduced the amplitude of the default calcium transient to 67% of its value to match our measurements in hiPSC-CMs.

Stem cell line derivation

R92Q stem cells were derived and the quality control was performed using procedures described in depth previously (Clippinger et al., 2019). Briefly, the parent human BJ fibroblast stem cell line (ATCC; BJFF.6) was reprogrammed to stem cells by the Genome Engineering and iPSC Center (GEiC) at Washington University in St. Louis. Two independent isogenic stem cell lines with the R92Q hTNNT2 point mutation were also generated at the GEiC using the CRISPR-Cas9 system (Jinek et al., 2012; Fig. S2). The oligo used to generate the guide RNA (gRNA) was 5′-CCTTCTCCATGCGCTTCCGGNGG-3′, and the mutation was introduced by homology-directed repair. This gRNA was selected to minimize off-target effects. The presence of the homozygous mutation was verified by sequencing. Karyotype (G-banding) analysis was performed by Cell Line Genetics (Fig. S2). Mycoplasma testing and immunofluorescence staining for pluripotency markers were performed by the GEiC (Fig. S3).

Stem cell and hiPSC-CMs culture

Stem cell culture and differentiation to hiPSC-CMs were done as previously described (Clippinger et al., 2019). Briefly, stem cells were maintained in feeder-free culture. To differentiate the stem cells to hiPSC-CMs, we used small-molecule manipulation of WNT signaling (Lian et al., 2012; Lian et al., 2013). hiPSC-CMs were enriched using metabolic selection (Sharma et al., 2015). All functional experiments were conducted at least 30 d after the initiation of differentiation. Experiments were conducted using two independently derived cell lines for the R92Q mutant. All experiments were repeated using at least two independent differentiations.

Microcontact patterning of hiPSC-CMs on glass and hydrogels

Fabrication of rectangular (7:1 aspect ratio) polydimethylsiloxane stamps for micropatterning of hiPSC-CMs on both glass and 10-kPa hydrogels was done as previously described (Ribeiro et al., 2015; Clippinger et al., 2019). Cells were patterned onto 10-kPa polyacrylamide hydrogels containing stamped Geltrex (Thermo Fisher Scientific) in rectangular patterns as reported previously (Clippinger et al., 2019; Fig. S3).

Quantification of troponin I isoform expression by Western blotting

Cell lysates from multiple differentiations were extracted from wild type and mutant hiPSC-CMs using protein lysis buffer containing 20 mM HEPES, pH 7.0, 150 mM NaCl, 0.5% 3-(3-cholamidopropyl)diethylammonio-1 propanesulfonate, and one protease inhibitor cocktail tablet (Roche complete mini EDTA-free tablets). 30 µg of each protein lysate was loaded per well of an Any kD Mini-PROTEAN TGX Precast Protein Gel (Bio-Rad), separated by electrophoresis, and transferred to polyvinylidene difluoride membranes (Sigma). Membranes were blocked with 5% milk and incubated overnight with primary antibodies. One membrane was incubated with mouse anti-GAPDH antibody (DSHB; DSHB-hGAPDH-2G7; 3 µg/ml) and mouse anti-slow skeletal troponin I antibody (Santa Cruz Biotechnology; sc-514899; 1:700). The other membrane was incubated with mouse anti-GAPDH antibody (DSHB; DSHB-hGAPDH-2G7; 3 µg/ml) and rabbit anti-cardiac troponin I (Santa Cruz Biotechnology; sc-15368; 1:500). After washing off the primary antibodies, the membranes were incubated with anti-rabbit IgG, HRP-linked antibody (Cell Signaling; 7074S; 1:2,000) and/or anti-mouse IgG, HRP-linked antibody (Cell Signaling; 7076S; 1:2,000). The proteins were detected using the SuperSignal West Dura Extended Duration Substrate (Thermo Fisher Scientific) and imaged on a MyECL Imager (Thermo Fisher Scientific). Blot intensity was quantified by densitometry using ImageJ (Schindelin et al., 2012; Fig. S4). P values were calculated using a Mann–Whitney *U* test.

Traction force microscopy

Traction force microscopy was conducted on 10-kPa hydrogels with cells patterned on rectangular patterns as previously described (Clippinger et al., 2019) and analyzed using the computational tool developed in Ribeiro et al., 2017. Data were analyzed, and 95% confidence intervals of the mean were calculated as described previously (Barrick et al., 2019; Clippinger et al., 2019). Briefly, the data were resampled using a bootstrapping algorithm to calculate 95% confidence intervals, and P values were calculated from the overlap regions between the distributions of bootstraps (Efron, 1979; Press, 1992; Martin, 2007; Barrick et al., 2019). Videos of contracting cells (Video 1) and sample traces derived from those videos (Fig. S5) are provided. Two independently derived cell lines were examined (Fig. S6).

Downloaded from http://rupress.org/jgp/article-pdf/153/5/e202012787/1413510/jgp_202012787.pdf by Washington University In St. Louis Libraries user on 01 May 2021

Measurement of calcium transients in live cells

Live-cell imaging was conducted using the ratiometric fluorescent calcium indicator dye Fura Red AM (Thermo Fisher Scientific). The use of a ratiometric dye is important since the mutation could affect the uptake of dye into the cells, and the ratiometric dye normalizes the calcium-induced changes in fluorescence to the total amount of dye taken up by the cell. hiPSC-CMs were patterned on hydrogels as described above. After 5–7 d on the patterns, the cells were loaded with 10 µM Fura Red AM dye and 0.01% Pluronic F-127 (Invitrogen/Thermo Fisher Scientific) in RPMI-B27 with insulin media for 20 min at room temperature. The cells were washed twice and incubated with Tyrode's solution (1.8 mM $CaCl_2$, 135 mM NaCl, 4 mM KCl, 1 mM $MgCl_2$, 5 mM glucose, and 10 mM HEPES, pH 7) for 15–20 min at 37°C to allow de-esterification of the dye. Calcium transients were recorded with a Nikon A1Rsi confocal microscope in line scan mode using a 40× objective and the Ex2Em1 microscope setting. Fura Red AM loaded cells were excited at both 405 nm and 488 nm, and the emission fluorescence signal was collected at 595 nm. Line scans were acquired at a sampling rate of 512 pixels × 1.9 ms per line (total 10,000 lines per recording). Each cell was recorded along with a line scan of the background fluorescence outside the cell area.

Analysis of calcium transients

The calcium transient fluorescence counts were converted to ratios using Fiji software (Schindelin et al., 2012). The averaged background fluorescence was subtracted from each recording and a montage was created from the image stacks. The ratio of fluorescence at 405 nm/488 nm was then calculated in Excel. The resulting ratiometric calcium fluorescence traces were then analyzed using a custom MATLAB script to calculate the amplitude of the calcium transient. Traces with fewer than three peaks were not analyzed. Briefly, the data were smoothed over a 100-point sliding window using a Savitsky–Golay filter. The locations of peaks and minima in the fluorescence signal were determined using a peak-finding algorithm. Statistical significance was tested using a two-tailed Student's *t* test.

Measurement of the expression of transcripts encoding key calcium-handling proteins

hiPSC-CMs were grown on Matrigel-coated (Corning) 10-kPa PrimeCoat elastic substrate culture dishes (ExCellness Biotech; 35 mm) for 10 d. Total RNA was isolated using RNeasy Mini Kit (Qiagen) with on-column DNase I treatment according to the manufacturer's instructions. cDNA was generated using iScript Reverse Transcription Supermix (Bio-Rad) according to the manufacturer's instructions. Quantitative PCR (qPCR) reactions were performed in triplicate using iTaq Universal SYBRGreen Supermix (Bio-Rad) and the ViiA 7 System (Applied Biosystems). Primers for all genes were obtained from IDT PrimeTime qPCR primers. Primer product numbers from IDT are listed in Table S1. Three separate biological samples were evaluated for both WT and R92Q homozygous hiPSC-CMs. The relative levels of mRNA were calculated using the comparative threshold cycle (ΔCt) method (Livak and Schmittgen, 2001). GAPDH and HPRT1 were used as endogenous controls, and Rox dye present in the master mix was used to normalize background fluorescence. ΔCt values are presented in Table S2. The statistical significance of differences in ΔCt values was evaluated using a Mann–Whitney *U* test.

Cellular electrophysiological studies

Whole-cell current- and voltage-clamp recordings were obtained at room temperature (~22–24°C) from hiPSC-CMs plated on hydrogel-coated coverslips using a Dagan 3900A (Dagan Corporation) amplifier interfaced to a Digidata 1332A A/D converter (Axon) and the pClamp 10.3 software (Axon). For current-clamp recordings, recording pipettes contained 135 mM KCl, 5 mM K_2ATP, 10 mM EGTA, 10 mM HEPES, and 5 mM glucose (pH 7.2; 310 mOsm). The bath solution contained 136 mM NaCl, 4 mM KCl, 2 mM $MgCl_2$, 1 mM $CaCl_2$, 10 mM HEPES, and 10 mM glucose (pH 7.4; 300 mOsm). For recordings of voltage-gated Ca^{2+} currents (I_{Ca}), pipettes contained 5 mM NaCl, 90 mM Cs CH_3SO_3, 20 mM CsCl, 4 mM MgATP, 0.4 mM Tris-GTP, 10 mM EGTA, 10 mM HEPES, and 3 mM $CaCl_2$ (pH 7.2; 310 mOsm), and the bath solution contained 20 mM NaCl, 110 mM TEA-Cl, 10 mM CsCl, 1 mM $MgCl_2$, 1 mM $CaCl_2$, 10 mM HEPES, and 10 mM glucose (pH 7.4; 300 mOsm). In all experiments, pipette resistances were 2–3 MΩ.

Electrophysiological data were acquired at 10 or 100 kHz, and signals were low pass filtered at 5 kHz before digitization and storage. After the formation of a gigaohm seal (>1GΩ) and establishment of the whole-cell configuration, brief (10 ms) ±5-mV voltage steps from a holding potential (HP) of −70 mV were presented to allow measurements of whole-cell membrane capacitance (C_m), input resistance (R_{in}), and series resistance (R_s). Mean ± SEM C_m values were 32 ± 2 pF and 47 ± 2 pF ($P < 0.001$) in WT ($n = 96$) and R92Q ($n = 67$) hiPSC-CMs, respectively. R_{in} values were 1,665 ± 125 MΩ and 1,551 ± 162 MΩ ($P > 0.05$) in WT ($n = 96$) and R92Q ($n = 67$) hiPSC-CMs, respectively. Whole-cell C_m and R_s values were electronically compensated by 85%. Voltage errors resulting from the uncompensated R_s were always <2 mV and were not corrected. Leak currents were always <50 pA and also were not corrected.

In current-clamp recordings, spontaneous action potentials were recorded on establishing the whole-cell configuration. To record evoked action potentials, small (approximately −10 to −100 pA) current injections were made to hyperpolarize the membrane potential to −80 mV and to stop spontaneous firing. Individual action potentials were then evoked by brief (4 ms) depolarizing current (600 pA) injections. In voltage-clamp experiments, whole-cell I_{Ca}, evoked in response to depolarizing (300 ms) voltage steps to test potentials between −45 and +15 mV (in 5-mV increments at 1-s intervals) from a HP of −50 mV, were recorded.

Analysis of electrophysiological data

Electrophysiological data were compiled and analyzed using Clampfit 10.3 (Axon) and GraphPad (Prism). C_m values were determined by integration of the capacitive transients recorded during ±5-mV voltage steps from −70 mV. Current amplitudes in each cell were normalized to the C_m, and current densities are reported (pA/pF). All data are presented as means ± SEM. The statistical significance of observed differences between WT and R92Q hiPSC-CMs was evaluated using two-tailed Student's *t* test or two-way ANOVA; P values are presented in Table S3.

Downloaded from http://rupress.org/jgp/article-pdf/153/5/e202012787/1413510/jgp_202012787.pdf by Washington University In St. Louis Libraries user on 01 May 2021

Online supplemental material

Fig. S1 shows the affinity of calcium binding to the troponin complex at 20°C and 37°C. Fig. S2 shows the generation of gene-edited hiPSC-CMs. Fig. S3 shows immunofluorescence images of stem cells and hiPSC-CMs. Fig. S4 shows the relative expression of fetal (slow skeletal) and adult (cardiac) troponin I isoforms in hiPSC-CMs. Fig. S5 shows representative traces of hiPSC-CMs spontaneously beating on 10-kPa polyacrylamide gels measured by traction force microscopy. Fig. S6 shows comparison of the two independently derived R92Q clones examined using traction force microscopy, revealing no significant differences between the clones. Table S1 displays quantitative reverse transcription PCR (RT-qPCR) gene names and primers. Table S2 lists RT-qPCR measurements of the expression of key calcium-handling genes. Table S3 presents values from the electrophysiological experiments in this study. Video 1 shows the displacement of beads by WT and R92Q hiPSC-CMs contracting on a 10-kPa polyacrylamide gel. This video was used to generate the representative traces in Fig. S5.

Results

Determination of the molecular mechanism of R92Q

At the molecular scale, the initial insult that drives the disease pathogenesis is mutation-induced alterations in protein function. Therefore, we set out to determine the molecular mechanism of the R92Q mutation in troponin T. WT and R92Q human troponin T were expressed and reconstituted into functional troponin complexes for biochemical and biophysical measurements. All assays were conducted using recombinant human tropomyosin and troponin complex. β-Cardiac ventricular myosin (*MYH7*) and cardiac actin were purified from porcine hearts. The porcine β-cardiac myosin isoform has 98% sequence identity with adult human β-cardiac ventricular myosin and similar biophysical properties, including indistinguishable ATPase kinetics and mechanics measured in the optical trap (Deacon et al., 2012; Greenberg et al., 2014; Sung et al., 2015).

We examined the effect of the R92Q mutation on thin filament regulation using an in vitro motility assay. In this assay, fluorescently labeled reconstituted regulated thin filaments are translocated over a bed of myosin in the presence of ATP and varying concentrations of calcium. The speed of translocation was measured as a function of calcium concentration, and normalized data were fitted with the Hill equation, as previously described (Greenberg et al., 2010). R92Q-regulated thin filaments show a shift in the pCa_{50} toward activation at submaximal, but physiologically relevant, calcium concentrations ($P < 0.001$; Fig. 2 A). There is no change in cooperativity, as determined by the Hill coefficient ($P = 0.76$).

The R92Q mutation does not change myosin detachment kinetics or calcium binding affinity

The shift toward submaximal calcium activation observed for R92Q in the in vitro motility assay stems from changes in the function of the troponin T protein. Given the role of troponin T in regulating calcium-dependent muscle contraction, three models have been proposed to explain the molecular mechanism of the R92Q mutation (Fig. 1 B): (1) R92Q could affect the cycling kinetics of myosins that are bound to the thin filament (Ford et al., 2012). In this model, one would expect to observe a change in the amount of time that myosin remains bound to the thin filament during cross-bridge cycling in the mutant. (2) R92Q could increase the calcium affinity of the troponin complex, leading to altered calcium buffering by myofilaments that directly disrupts calcium homeostasis (Schober et al., 2012; Ferrantini et al., 2017; Robinson et al., 2018). In this model, one would expect to observe an increased binding affinity for calcium in the troponin complex containing R92Q. (3) R92Q could alter the distribution of positions assumed by tropomyosin along the thin filament, leading to changes in the fraction of bound myosin cross-bridges (McConnell et al., 2017). In this model, one would expect to see changes in the equilibrium constants that define the positioning of tropomyosin along the thin filament. We set out to test these three models.

First, we tested whether the mutation affects the kinetics of myosin detachment from the thin filament by using stopped-flow kinetics to measure the rate of ADP release from actomyosin (i.e., the transition that limits actomyosin dissociation and unloaded sliding velocity), as we have done previously (Clippinger et al., 2019). We found that the rate of ADP release from myosin bound to regulated thin filaments is not affected by the R92Q mutation ($P = 0.88$; Fig. 2 B). Therefore, changes in myosin detachment kinetics cannot explain the shift toward submaximal calcium activation seen in the in vitro motility assay.

We measured whether the calcium binding affinity to the troponin complex is affected by the mutation. We used an IAANS-labeled form of troponin C to characterize calcium binding to the troponin complex (Robinson et al., 2007; Liu et al., 2012). The fluorescence intensity of this probe changes upon calcium binding to troponin C (Davis et al., 2007; Robinson et al., 2007; Liu et al., 2012; Williams et al., 2016). We used it to spectroscopically measure the affinity of calcium binding to regulated thin filaments (Fig. 2 C; Liu et al., 2012). We saw that the calcium concentration required for half-maximal activation is not significantly different for the WT and R92Q mutant proteins ($P = 0.93$). Similar results were seen at 15°C (Fig. 2 C), 20°C, and 37°C (Fig. S1). These results demonstrate that changes in the affinity of calcium binding to troponin C cannot explain the shift toward submaximal calcium activation seen in the in vitro motility assay (Fig. 2 A). Our finding of no change in calcium affinity for troponin C is consistent with some (Liu et al., 2012), but not all (Robinson et al., 2007), previous studies. The difference between our results and those obtained in previous studies showing changes in calcium affinity could come from differences in the calcium-sensing troponin constructs used, the actin proteins used (i.e., skeletal [Robinson et al., 2007] versus cardiac in the present study), or possibly other experimental conditions, such as the buffer composition.

The initial biophysical insult of R92Q is increased thin filament activation due to repositioning of tropomyosin along the thin filament

To test whether the shift in calcium sensitivity can be explained by a change in the distribution of positions assumed by tropomyosin along the thin filament (Fig. 3 A), we measured the equilibrium constants that define the fraction of thin filament regulatory units in each state (McKillop and Geeves, 1993;

Downloaded from http://rupress.org/jgp/article-pdf/153/5/e202012787/1413510/jgp_202012787.pdf by Washington University In St. Louis Libraries user on 01 May 2021

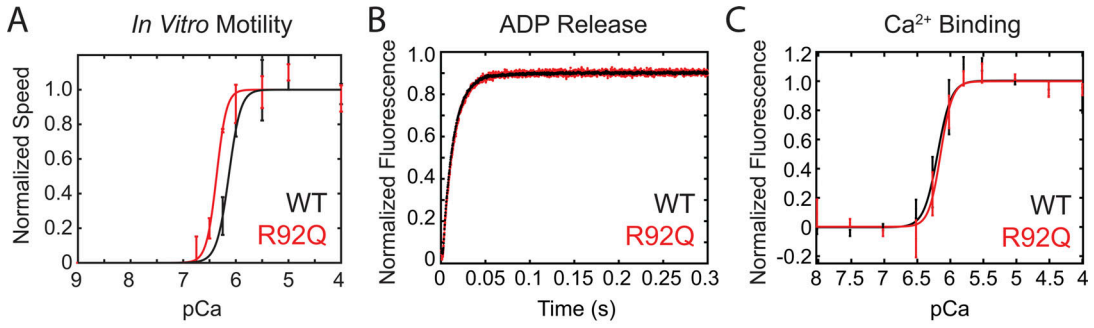

	WT	R92Q	p
Motility pCa50 (n=3)	6.12 (±0.02)	6.37 (±0.03)	<0.001
Motility Hill (n=3)	3.8 (±0.6)	3.4 (±0.7)	0.75
ADP release (s^{-1}) (n=4)	76.3 (±5.0)	75.8 (±3.9)	0.88
IAANs Ca50 (μM) (n=5)	0.66 (±0.18)	0.67 (±0.19)	0.93
IAANs Hill (n=5)	2.69 (±0.40)	3.50 (±0.39)	0.01

Figure 2. **R92Q does not change the rate of unloaded actomyosin dissociation or calcium binding affinity to troponin C. (A)** In vitro motility assays using cardiac myosin and reconstituted regulated thin filaments. The speed of motility was measured as a function of calcium. R92Q shows a shift toward submaximal calcium activation. WT data are from Clippinger et al. (2019). Error bars represent SDs from three separate experiments. **(B)** The rate of ADP release from myosin attached to regulated thin filaments was measured using stopped-flow kinetics (fluorescence transients are shown). Myosin bound to ADP and pyrene-labeled regulated thin filaments was rapidly mixed with ATP, and the fluorescence increases as myosin dissociates from the thin filament. The rate of actomyosin dissociation was unchanged by the R92Q mutation. WT data are from Clippinger et al. (2019). Curves show the average of five technical repeats. **(C)** The affinity of calcium binding to the troponin complex. IAANS-labeled troponin C was reconstituted into regulated thin filaments. Titrations with increasing calcium were conducted, and there is no difference in calcium binding affinity between WT and R92Q. Error bars show the SD of five experiments. Values derived from fits, standard errors in the fits, and P values are shown. P values were calculated using a two-tailed Student's *t* test.

Barrick et al., 2019). The equilibrium constant between the blocked and closed states, K_B, was determined by rapidly mixing fluorescently labeled regulated thin filaments together with myosin and then measuring the rate of myosin binding (seen as quenching of the fluorescence signal) in the presence and absence of calcium (see Materials and methods for details). At low calcium, when tropomyosin is primarily in the blocked state, the rate of myosin binding to the thin filament is slower than at high calcium, when the blocked state is less populated. The ratio of the rates of binding at low and high calcium were used to calculate K_B (Eq. 1 and Fig. 3 B). As can be seen from the fluorescence transients, the rate of myosin binding to regulated thin filaments is similar for the WT and R92Q mutant proteins at high calcium (pCa 4); however, at low calcium (pCa 9), the rate of binding for the mutant is much faster than for the WT, consistent with lower population of the blocked state. When we calculate K_B, we see that it is significantly larger in the mutant compared with the WT (P = 0.003), meaning that population of the more inhibitory blocked state is reduced while population of the closed state is increased. The increased K_B value means that, at low calcium levels, the thin filament will be more activated in the mutant, consistent with the in vitro motility measurements (Fig. 2 A).

Next, we considered whether the mutation affects the equilibrium constant for the transitions between the closed and open states, K_T, or the equilibrium constant between the open and myosin weakly bound states, K_w. To do this, we performed titrations of fluorescently labeled regulated thin filaments with increasing concentrations of myosin and measured the quenching of the fluorescence as the myosin binds to the regulated thin filaments (Fig. 3 C). These data, analyzed using a modification of the method of McKillop and Geeves (McKillop and Geeves, 1993; Barrick et al., 2019), show that there are no significant differences in K_T between WT and R92Q (Fig. 3). There is a small increase in K_w; however, its magnitude is insufficient to explain the shift in the in vitro motility assay. This demonstrates that the primary molecular defect in R92Q is partial activation of the thin filament at low calcium levels due to reduced population of the inhibitory blocked state. Taken together, our results demonstrate that the initial molecular insult resulting from the R92Q mutation is decreased population of the thin filament blocked state, leading to increased thin filament activation and myosin-driven force generation.

Computational modeling corroborates the assertion that altered tropomyosin positioning with R92Q is sufficient to explain the shift toward submaximal calcium activation

To model the effects of the initial molecular insult identified in our biochemical studies, we utilized a widely used computational model of thin filament activation that was originally developed by Campbell et al. (Campbell et al., 2010). This model is based on the McKillop and Geeves three-state formalism that was also used to analyze our data (McKillop and Geeves, 1993). In this model, the equilibrium constants for transitions between thin filament states are inputted, and the model predicts several parameters, including the force per sarcomere as a function of calcium. When we used the default parameters of the model but proportionally increase the value of K_B to match the fractional change seen in our biochemical experiments with the mutant (Fig. 4 A), we find that this change alone is sufficient to produce

Downloaded from http://rupress.org/jgp/article-pdf/153/5/e202012787/1413510/jgp_202012787.pdf by Washington University In St. Louis Libraries user on 01 May 2021

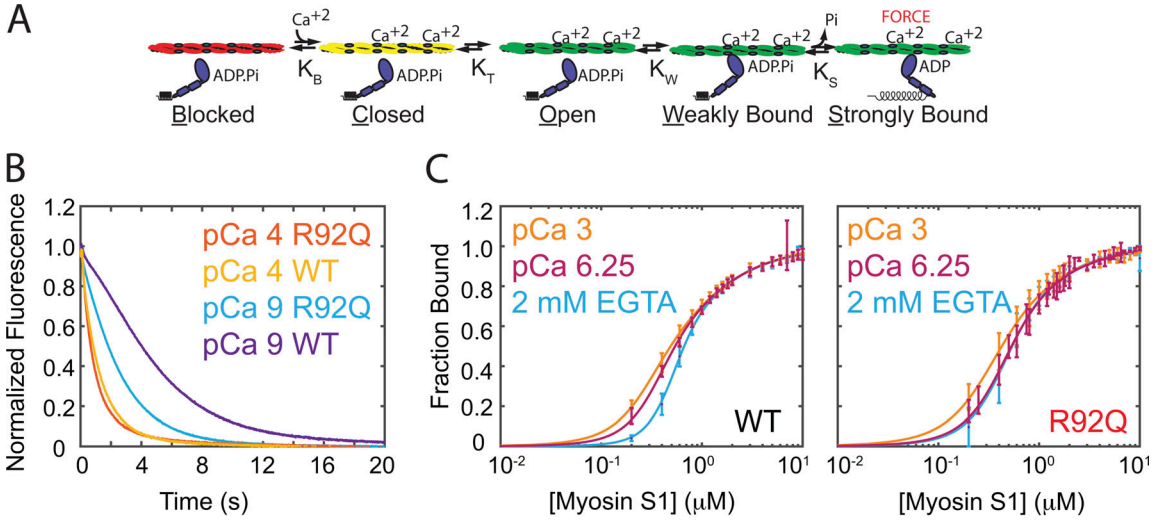

	WT	R92Q	p
K_B	0.40 (-0.15/+0.15)	1.02 (-0.26/+0.26)	0.003
K_W	0.13 (-0.01/+0.01)	0.18 (-0.04/+0.22)	0.014
K_T 2mM EGTA	0.06 (-0.03/+0.06)	0.13 (-0.10/+0.10)	0.39
K_T pCa 6.25	0.08 (-0.04/+0.04)	0.08 (-0.06/+0.05)	0.75
K_T pCa 3	0.18 (-0.07/+0.08)	0.21 (-0.15/+0.16)	0.94
Cooperativity (n)	5.97 (-0.95/+1.35)	4.01 (-1.69/+3.20)	0.20

Figure 3. **R92Q alters the positioning of tropomyosin along the thin filament. (A)** Kinetic scheme for thin filament activation. **(B)** Measurement of the equilibrium constant K_B using stopped-flow kinetics methods (fluorescence transients are shown). Pyrene-labeled regulated thin filaments were rapidly mixed with myosin at high (pCa 4) or low (pCa 9) calcium, and the rate of myosin binding was measured by quenching of the fluorescence. K_B is calculated as described in Materials and methods. The rate of myosin binding is similar for the WT and R92Q at pCa 4 but much faster for R92Q at pCa 9, consistent with destabilization of the blocked state. K_B for R92Q is significantly larger than the WT. **(C)** Measurement of the parameters K_T and K_W using equilibrium titrations of myosin with regulated thin filaments. Fitting reveals no significant differences for R92Q for either K_T or K_W compared with the WT. WT data are from Clippinger et al. (2019). Error bars show the standard deviation of five experiments. The average value, 95% confidence intervals calculated from bootstrapping, and P values derived from the distribution of bootstrapped values are shown in the table.

the shift toward submaximal calcium activation observed in the in vitro motility experiments (Fig. 2 A).

Generation of gene-edited stem cell–derived cardiomyocytes

To examine the effects of the R92Q mutation in human cells, we used CRISPR-Cas9 to generate two independent hiPSC lines that are homozygous for the R92Q mutation (Fig. S2). While there are several splice isoforms of troponin T expressed during development, the primary isoform expressed in hiPSC-CMs is the adult isoform (Cai et al., 2019). All of these isoforms contain R92, so all of the troponin T expressed in the cell has the mutation (Fig. S2). Homozygous lines were used to facilitate direct correlation of the molecular insult with alterations in cellular function. Heterozygous lines would better mimic the disease seen in humans but would contain complex mixtures of WT and mutant proteins, confounding the correlation of the molecular and cellular results. Both WT and R92Q hiPSCs were derived from the same parent line and are therefore isogenic except for the mutation. We previously showed, by whole-exome sequencing of the parent line, that it has no known variants associated with cardiomyopathy (Clippinger et al., 2019). Gene-edited hiPSCs are pluripotent, as assessed by immunofluorescence (Fig. S3 A), and have normal karyotypes (Fig. S3 B). hiPSCs were differentiated to hiPSC-CMs through temporal modulation of WNT signaling (Lian et al., 2012), and our efficiency of differentiation using this procedure is >90% (Clippinger et al., 2019). Both WT and R92Q cells express similar ratios of fetal (slow skeletal) to adult (cardiac) troponin I isoforms (P = 0.49; Fig. S4).

R92Q hiPSC-CMs generate increased force, power, and contraction speed compared with WT cells

To test whether R92Q hiPSC-CMs show the altered contractility seen in some model systems, we measured the contractility of single hiPSC-CMs using traction force microscopy. hiPSC-CMs were seeded onto rectangular extracellular matrix patterns on polyacrylamide hydrogels of physiological stiffness (10 kPa; Clippinger et al., 2019). This patterning on physiological stiffness hydrogels promotes hiPSC-CM maturation and sarcomeric alignment (Ribeiro et al., 2015). Patterned hiPSC-CMs show sarcomeres that align preferentially along the long axis of the cell (Fig. S3 B), and these cells contract primarily along that single axis (Video 1). The force, speed of contraction, and power were calculated from the displacement of beads embedded in the hydrogel (Fig. S5; Ribeiro et al., 2017). Data were plotted as

Downloaded from http://rupress.org/jgp/article-pdf/153/5/e202012787/1413510/jgp_202012787.pdf by Washington University In St. Louis Libraries user on 01 May 2021

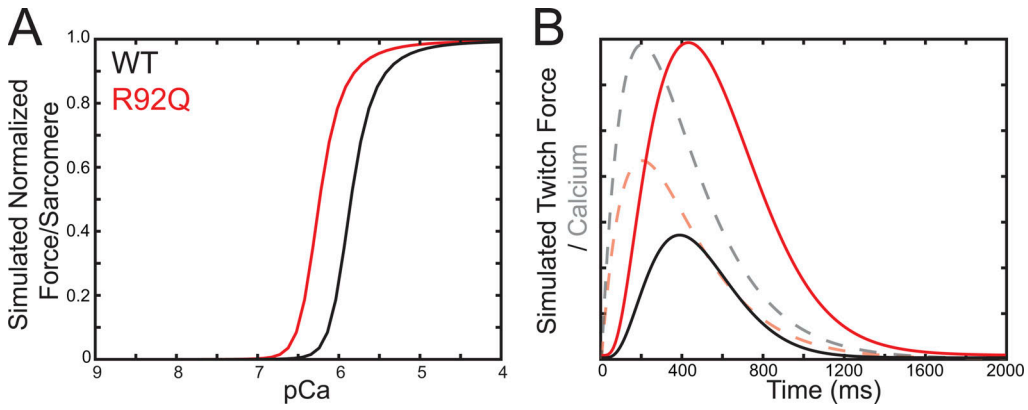

Figure 4. **Computational modeling reveals that altered tropomyosin positioning is sufficient to explain the hypercontractility seen with R92Q. (A)** Using the computational model developed by Campbell et al. (2010) and the measured equilibrium constants for thin filament activation, the steady-state force per sarcomere was calculated. Changing K_B alone is sufficient to reproduce the shift toward submaximal calcium activation seen in the in vitro motility experiments (Fig. 2 A). **(B)** Using the same model, the equilibrium constants measured in vitro, and the calcium transients measured in hiPSC-CMs (Fig. 6 A), the twitch force (solid line) in response to a calcium transient (dashed line) was calculated. Consistent with our cellular measurements, the simulations demonstrate that despite having a reduced calcium transient, R92Q produces a larger force in a twitch due to changes in tropomyosin positioning.

cumulative distributions of single cells to account for cell-to-cell variability (Clippinger et al., 2019). R92Q hiPSC-CMs generate more force and power and have a higher contractile speed compared with the WT (Fig. 5). There were no significant differences observed between the two independently derived R92Q clones that we examined (Fig. S6).

Intracellular calcium transients are reduced in R92Q cells

While the initial molecular insult driving the disease pathogenesis is alterations in tropomyosin positioning, which increases molecular contractility, changes in contractility can lead to downstream activation of adaptive and maladaptive pathways. Previous studies using transgenic mice with troponin T mutations also showed altered cardiomyocyte calcium handling (Rice et al., 2010; Schober et al., 2012; Coppini et al., 2017; Ferrantini et al., 2017; Robinson et al., 2018). To examine calcium dynamics in hiPSC-CMs, cells were patterned onto rectangular ECM patterns on 10-kPa hydrogels and loaded with the ratiometric fluorescent calcium indicator dye Fura Red. Line scans of the fluorescence of spontaneously beating cells were collected at 1.9-ms intervals. As can be seen, hiPSC-CMs display well-defined calcium transients (Fig. 6 A); however, the amplitudes of the transients are lower ($P < 0.002$) in R92Q (0.56 ± 0.13; n = 18) compared with WT (0.84 ± 0.11; n = 19) cells. Although the low signal-to-noise ratio of the dye on the hydrogel substrate precluded us from determining whether there were differences in diastolic calcium, as has been reported previously (Schober et al., 2012; Robinson et al., 2018), the data presented demonstrate that despite generating increased force, R92Q hiPSC-CMs have reduced calcium transient amplitudes compared with WT cells.

To see whether the reduced population of the blocked state, observed in our molecular studies (Fig. 4 B), is sufficient to explain the hypercontractility seen in cells despite the reduction in calcium transient amplitude, we used the same computational model described earlier to predict the force per sarcomere in response to a calcium transient. In the modeling, the amplitude of the calcium transient for R92Q was reduced to 67% of the value seen in the WT, as observed in our cellular measurements (Fig. 6 A). As above, we proportionally increased K_B for the mutant to match the relative difference seen in our biochemical experiments. Consistent with our cellular experiments, the model predicts that the mutant will generate more force in response to a calcium transient than the WT, despite having a smaller amplitude calcium transient (Fig. 4 B). It should be noted that hiPSC-CMs express complex mixtures of fetal and adult protein isoforms and that, as a result, there could be some subtle differences between the absolute forces predicted by the model, which is based on the equilibrium constants measured for the adult proteins, and the experimentally measured forces in hiPSC-CMs.

R92Q cells show alterations in expression of calcium-handling genes

The observed changes in calcium handling could come from a variety of sources, including changes in transcription, protein expression, and/or posttranslational modifications of proteins that regulate calcium homeostasis. To explore a possible role for transcriptional remodeling downstream of the initial molecular insult, we performed RT-qPCR analyses of the expression of transcripts encoded by key genes involved in the regulation of calcium homeostasis in cardiomyocytes (Fig. 6). Specifically, we examined the expression levels of transcripts encoding phospholamban (*PLN*), sarcoendoplasmic reticulum calcium-ATPase (*ATPA2*), voltage-gated calcium channel subunits (*CACNA1C*, *CACNA1G*, and *CACNA1H*), inositol triphosphate receptor (*ITPR2*), calsequestrin (*CASQ2*), calcium-calmodulin dependent kinase 2 (*CAMK2D*), sodium-calcium exchanger (*SLC8A1*), and the ryanodine receptor (*RYR2*). We found marked up-regulation of *CASQ*, *CAMK2D*, and *SLC8A1* and down-regulation of *CACNA1H* in R92Q compared with WT hiPSC-CMs (Figs. 6 B, Table S1, and Table S2), demonstrating that the expression levels of key genes associated with calcium handling are altered in R92Q hiPSC-CMs.

Downloaded from http://rupress.org/jgp/article-pdf/153/5/e202012787/1413510/jgp_202012787.pdf by Washington University In St. Louis Libraries user on 01 May 2021

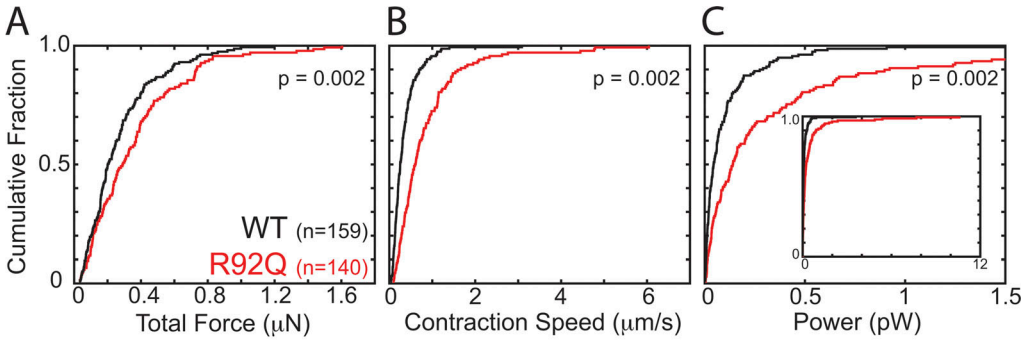

	WT (n=159)	R92Q (n=140)	p
Total force (μN)	0.27 (-0.03/+0.04)	0.36 (-0.04/+0.05)	0.002
Contraction speed (μm/s)	0.35 (-0.05/+0.06)	0.84 (-0.22/+0.23)	0.002
Contraction power (pW)	0.12 (-0.04/+0.06)	0.47 (-0.3/+0.3)	0.002

Figure 5. **R92Q causes cellular hypercontractility in hiPSC-CMs.** Single hiPSC-CMs were seeded on rectangular patterns on 10-kPa hydrogels for traction force microscopy. **(A–C)** Cumulative distributions reveal that R92Q hiPSC-CMs have a greater total force (A), contraction speed (B), and contraction power (C) compared with WT. WT data are from Clippinger et al. (2019). Values from the analysis, number of cells examined, 95% confidence intervals obtained from bootstrapping, and P values derived from the distributions of bootstrapped values are listed in the table.

R92Q cells show altered action potentials and reduced inward calcium current densities

The observed reductions in the calcium transients observed in spontaneously beating R92Q cells could reflect changes in transmembrane calcium influx. To determine directly if membrane excitability is altered in R92Q cells, we obtained whole-cell current-clamp recordings of spontaneous action potentials in WT and R92Q mutant hiPSC-CMs patterned onto rectangular ECM patterns on 10-kPa hydrogels (Fig. 7, A and B). Analyses of the data obtained in these experiments revealed that the maximum diastolic potential (the most negative membrane potential achieved between action potentials in spontaneously firing cells) is more depolarized in R92Q hiPSC-CMs than in WT hiPSC-CMs (Fig. 7 B). In

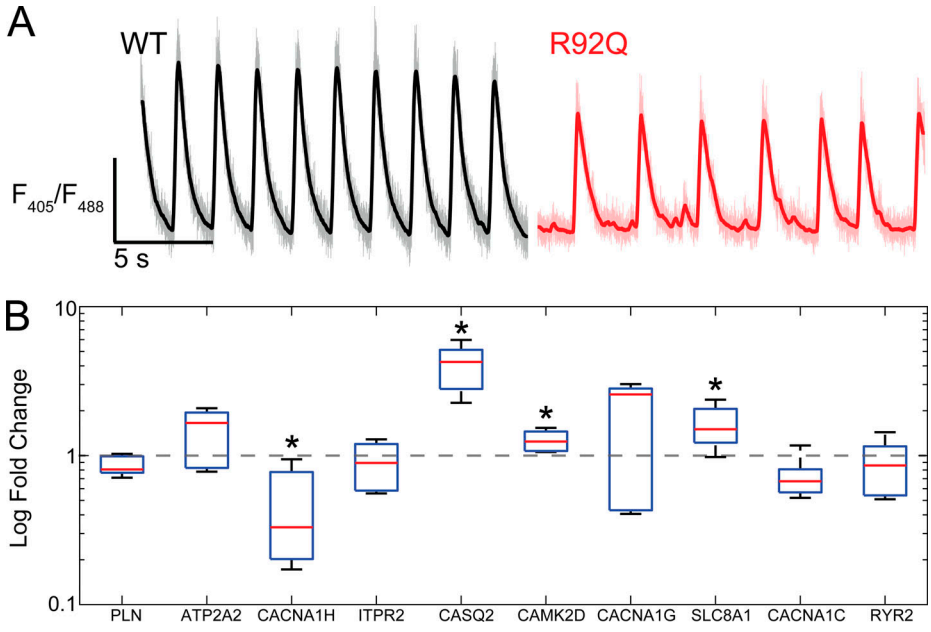

Figure 6. **R92Q hiPSC-CMs show altered calcium transients and gene expression. (A)** Representative fluorescence ratio traces showing calcium transients. Single hiPSC-CMs were seeded on rectangular patterns on 10 kPa hydrogels and loaded with the ratiometric calcium dye, Fura Red. R92Q hiPSC-CMs calcium transients have lower amplitudes than the WT cells. **(B)** Expression of key calcium-handling genes measured using qPCR. Data show significant increases in the expression of CASQ2, CAMK2D, and SLC8A1 and a decrease in CACNA1H. ΔCt values are shown in Table S2. Statistics were performed on the ΔCt values; however, we show the log-fold changes. Red lines show the means, boxes show the quartiles, and error bars show the standard deviations. Data shown reflect three biological replicates, each of which included three technical replicates. Asterisk denotes ΔCt values with $P < 0.05$ compared with the WT. P values were calculated using a Mann–Whitney test.

Downloaded from http://rupress.org/jgp/article-pdf/153/5/e202012787/1413510/jgp_202012787.pdf by Washington University In St. Louis Libraries user on 01 May 2021

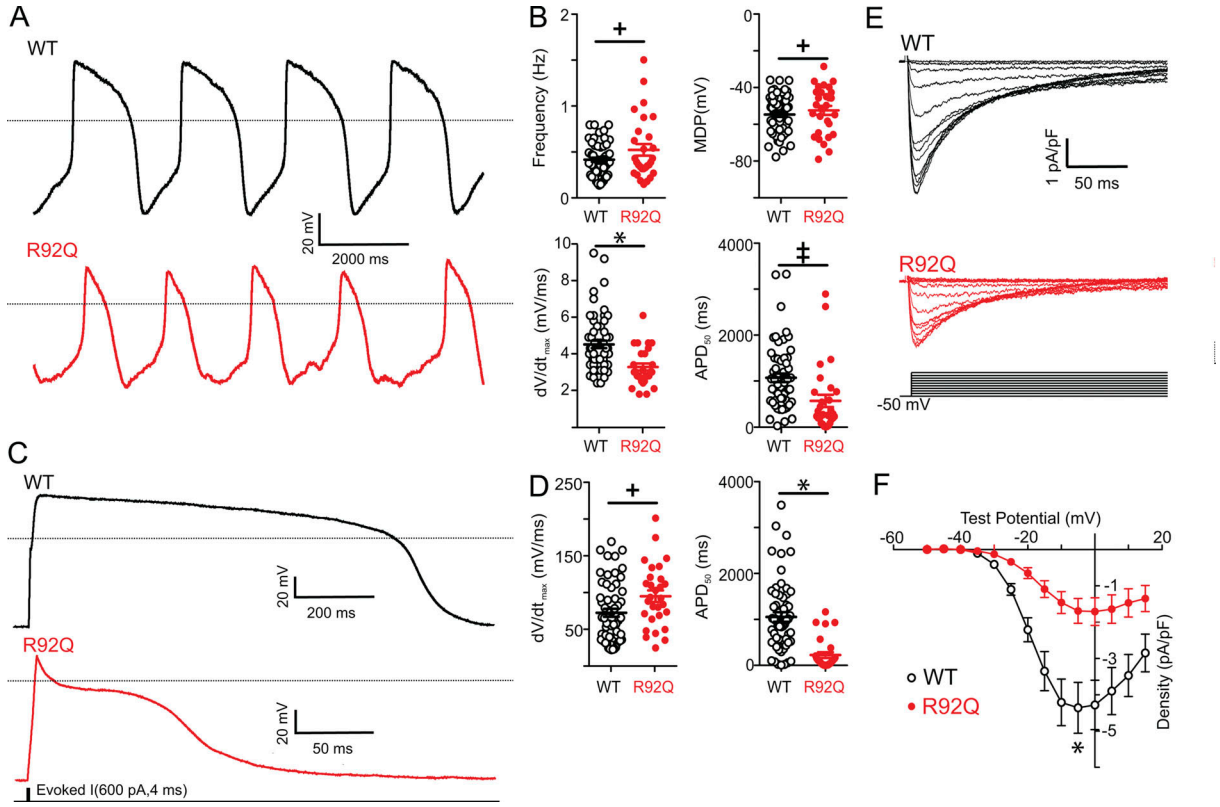

Figure 7. **Spontaneous and evoked action potentials are altered in R92Q hiPSC-CMs and I_{Ca} densities are reduced. (A)** Representative whole-cell spontaneous action potentials recorded from WT and R92Q hiPSC-CMs are illustrated; dotted black lines indicate 0 mV. **(B)** Firing frequencies, maximum diastolic potentials (MDP), maximum upstroke velocities (dV/dt_{max}) and APD_{50} measured in individual WT (n = 58) and R92Q (n = 29) hiPSC-CMs are plotted; mean values are also indicated and are provided in Table S3. **(C)** Representative whole-cell action potential waveforms evoked from a hyperpolarized membrane potential, as described in Materials and methods, in WT and R92Q cells are shown; dotted black lines indicate 0 mV. **(D)** dV/dt_{max} and APD_{50} values measured in individual WT (n = 58) and R92Q (n = 29) cells are plotted; mean values are also indicated and are provided in Table S3. **(E)** Representative voltage-gated Ca^{2+} current (I_{Ca}) waveforms, elicited by voltage steps to test potentials between −40 and +15 mV (in 5-mV increments) from a HP of −50 mV, in WT and R92Q hiPSC-CMs are shown. **(F)** Mean ± SEM peak I_{Ca} densities in R92Q (n = 12) and WT (n = 15) hiPSC-CMs are plotted as a function of the test potential. Values in R92Q mutant cells are significantly different from those in WT cells at the +, $P < 0.05$; ‡, $P < 0.01$; and *, $P < 0.001$ levels. P values were calculated using a two-tailed Student's t test.

addition, the frequency of spontaneous action potential firing is higher, upstroke velocities (i.e., the rate of membrane depolarization) are lower, and action potential durations at 50% repolarization (APD_{50}) are shorter in R92Q hiPSC-CMs compared with WT cells (Fig. 7 B and Table S3).

To better understand the mechanisms contributing to the reductions in the APD_{50} seen in spontaneously beating R92Q cells, we examined the waveforms of evoked action potentials of hiPSC-CMs hyperpolarized to a membrane potential of −80 mV. Although similar hyperpolarizing currents were required to render R92Q and WT hiPSC-CMs electrically silent and similar currents were required to evoke action potentials in WT and mutant cells, the durations of evoked action potentials are significantly shorter in R92Q cells than in WT cells (Fig. 7, C and D).

Additional voltage-clamp experiments were conducted to determine directly if voltage-gated inward calcium current densities were altered in R92Q compared with WT cells. With outward potassium currents blocked, we recorded whole-cell voltage-gated calcium currents evoked on membrane depolarization in WT and R92Q hiPSC-CMs. As illustrated in Fig. 7 E, these experiments revealed that inward calcium current densities are markedly reduced in R92Q compared with WT hiPSC-CMs (Fig. 7 F).

Discussion

Here, we elucidated the molecular and cellular consequences of the R92Q mutation in troponin T. We show that the initial molecular insult that drives disease pathogenesis is increased thin filament activation at physiologically relevant micromolar calcium levels due to destabilization of the tropomyosin blocked state. We demonstrate computationally and experimentally that this increased activation is consistent with the increased mechanical force produced by hiPSC-CMs. We show that altered mechanical forces lead to downstream changes in the expression of calcium-handling genes, altered calcium transients, and alterations in cellular electrophysiology. Taken together, our results highlight the role of mechanobiology in driving the early disease pathogenesis.

Defining the primary molecular driver of the disease pathogenesis

Previous studies demonstrated that R92Q mutant protein is expressed and properly integrated into sarcomeres, suggesting that the driver of the disease is changes in protein function rather than haploinsufficiency (Marian et al., 1997; Sweeney et al., 1998; Tardiff et al., 1999; Yanaga et al., 1999). Our results

Downloaded from http://rupress.org/jgp/article-pdf/153/5/e202012787/1413510/jgp_202012787.pdf by Washington University In St. Louis Libraries user on 01 May 2021

demonstrating that R92Q causes a shift toward submaximal calcium activation (Fig. 2 A) are consistent with some (Morimoto et al., 1998; Yanaga et al., 1999; Szczesna et al., 2000; Chandra et al., 2001; Robinson et al., 2002; Ford et al., 2012), but not all (Sweeney et al., 1998; Rust et al., 1999), previous measurements in muscle fibers and biochemical assays using noncardiac protein isoforms. The shift toward submaximal calcium activation could come from changes in actomyosin dissociation kinetics, the affinity of calcium binding to troponin C, and/or the positioning of tropomyosin along the thin filament (Fig. 1 B).

Our results demonstrate that R92Q does not affect the calcium binding affinity of troponin C or the kinetics of actomyosin dissociation (Fig. 2); however, the mutation increases the equilibrium constant between the blocked and closed states (Fig. 3 B). This change favors the closed state over the blocked state, lowering the energy barrier for thin filament activation at physiologically relevant calcium concentrations (pCa 5–7). Our computational modeling (Fig. 4) demonstrates that the increase in this equilibrium constant is sufficient to explain the shift toward submaximal calcium activation seen in our in vitro motility measurements (Fig. 2 A). Our data demonstrate that the initial insult that drives the early disease pathogenesis is reduced population of the inhibitory blocked position of tropomyosin at low calcium, which would lead to increased thin filament activation.

The R92Q mutation has been studied in many model systems, including quail myotubes (Sweeney et al., 1998), transfected rat cardiomyocytes (Rust et al., 1999), skinned rabbit muscle fibers (Morimoto et al., 1998), transgenic mice (Tardiff et al., 1999), and transfected cat cardiomyocytes (Marian et al., 1997). While these studies have greatly advanced our understanding of the mutation, they also demonstrated that the effects of the mutation depend on the model system used. Studies using transgenic mice demonstrated that disease presentation depends on whether proteins with biophysical properties similar to human isoforms are used (Ford et al., 2012). The use of all cardiac proteins with biophysical properties similar to human proteins is important for studies of thin filament mutations, since the activation of the thin filament depends on both myosin and calcium binding (Fig. 3 A). The most commonly used myosins in studies of R92Q mutation have been murine ventricular myosin (MYH6–92% sequence identity with human ventricular myosin) and rabbit fast skeletal muscle myosin (MYH2–82% sequence identity with human ventricular myosin), both of which have very different biophysical properties than human ventricular myosin (VanBuren et al., 1995; Malmqvist et al., 2004; Debold et al., 2007; Deacon et al., 2012). Our molecular studies used human cardiac troponin and tropomyosin and porcine cardiac myosin and actin. Porcine cardiac actin is identical in sequence to human cardiac actin. Porcine cardiac myosin (*MYH7*) is 98% identical in sequence to the human isoform and displays biochemical kinetics, mechanical step sizes, and load-dependent kinetics that are indistinguishable from human cardiac myosin (Deacon et al., 2012; Greenberg et al., 2014; Sung et al., 2015).

Interestingly, the R92 residue is in the region of troponin T that interacts with tropomyosin (Yamada et al., 2020). Two other HCM mutations have been identified at R92, R92W, and R92L, leading to the suggestion that R92 is a hotspot for HCM mutations. While there are no atomic-resolution structures of this region of the thin filament, structural studies have shown that troponin T plays a role in stabilizing the tropomyosin blocked state (Tobacman et al., 2002; Johnson et al., 2019; Madan et al., 2020). Molecular dynamics simulations demonstrated that mutations at R92 can change the distance between troponin T and tropomyosin (Manning et al., 2011), and biochemical experiments showed that R92L decreases the affinity of troponin for tropomyosin (Gangadharan et al., 2017). These two mechanisms are not mutually exclusive, and we speculate that R92Q reduces the coupling between troponin conformation and tropomyosin positioning, leading to destabilization of the blocked state. It is worth noting that we have focused on the effects of a troponin T mutation on calcium-based activation due to the central role of troponin in calcium-dependent thin filament regulation. Recent work has suggested that the N-terminal region of myosin binding protein C can play a role in activating the thin filament in the C-zone (Mun et al., 2014; Risi et al., 2018; Napierski et al., 2020). It will be interesting to investigate whether the R92Q mutation also affects the interactions of myosin binding protein C with the thin filament.

Recent studies of HCM-causing mutations in thick filament proteins, including β-cardiac myosin, myosin binding protein C, myosin regulatory light chain, and myosin essential light chain, have demonstrated that many of these mutations disrupt the autoinhibited super relaxed state of myosin, leading to the recruitment of more cross-bridges and thus to hypercontractility (Spudich, 2015; McNamara et al., 2016; Alamo et al., 2017; Nag et al., 2017; Adhikari et al., 2019; Sitbon et al., 2020). It has been proposed that increased cross-bridge recruitment correlates with the hyperdynamic cardiac function seen in HCM (Alamo et al., 2017). Our studies with R92Q, a thin filament mutation, demonstrate a similar net effect of increased cross-bridge recruitment at physiologically relevant calcium levels, suggesting that altered recruitment of cross-bridges in HCM as a common theme for both some thin and thick filament mutations.

It has been proposed that R92Q causes an increase in troponin C's calcium affinity, which would affect the buffering of calcium by myofilaments, disrupting calcium homeostasis (Schober et al., 2012; Robinson et al., 2018). While our cellular data reveal disrupted calcium homeostasis, our molecular experiments show no change in the affinity of calcium for R92Q troponin, demonstrating that disrupted calcium homeostasis is a downstream consequence of the initial molecular insult. Our results are consistent with the notion that the development of HCM correlates with changes in tension rather than calcium handling (Davis et al., 2016).

Connecting the molecular and cellular phenotypes in R92Q

R92Q hiPSC-CMs show both an increase in force production (Fig. 5 A) and a reduction in the amplitude of the calcium transient (Fig. 6 A). These seemingly conflicting findings can be reconciled by our computational modeling (Fig. 4 B), which predicts that the shift toward submaximal calcium activation observed at the molecular scale can lead to cellular hypercontractility, despite the reduction in the amplitude of the

Downloaded from http://rupress.org/jgp/article-pdf/153/5/e202012787/1413510/jgp_202012787.pdf by Washington University In St. Louis Libraries user on 01 May 2021

calcium transient. This hypercontractility occurs at physiologically relevant (micromolar) concentrations of calcium (Bers, 2002). Therefore, the observed cellular hypercontractility is consistent with the proposed molecular mechanism.

At the cellular level, we see disrupted calcium homeostasis with R92Q, which is downstream of the initial contractile insult. Calcium homeostasis in the myocardium is a complicated process that depends on many factors, including gene expression and posttranslational modifications of signaling and contractile proteins (Bers, 2002). While a complete dissection of this mechanism is beyond the scope of the current study, our results provide insights into potential transcriptional mechanisms. We observed changes in the expression of several genes involved in calcium handling (Fig. 6 B), including calsequestrin (*CASQ2*), calcium-calmodulin kinase (*CAMK2D*), the sodium-calcium exchanger (*SLC8A1*), and a voltage-gated calcium channel subunit (*CACNA1H*). Interestingly, overexpression of *CASQ2* or *CAMK2D* in transgenic mice causes heart failure and arrhythmogenesis (Sato et al., 1998; Zhang et al., 2003). While we recognize that changes in transcript expression do not always correlate with protein function, our data demonstrate that altered mechanics at the molecular level can drive changes in gene expression, showing a mechanobiological link between these processes in HCM. It is worth noting that some of the differentially expressed calcium-handling genes observed here in human cells are different from observations in the R92Q mouse model, which may be due to species differences (Coppini et al., 2017; Chowdhury et al., 2020). Interestingly, in mice, ablation of *PLN* can rescue the HCM phenotype, and it will be interesting to see whether similar results are observed in human cells (Chowdhury et al., 2020).

Our single-cell electrophysiological experiments reveal that action potential durations are shorter in R92Q, compared with WT cells, due in part to reduced inward L-type calcium current densities (Fig. 7). These changes would be expected to be arrhythmogenic and could contribute to the increased incidence of arrhythmias and sudden death in individuals harboring the mutation. We observe normal expression levels of the transcripts encoding L-type channel subunits, and therefore, the reduced current density could be due to alterations in signaling pathways and/or posttranslational modifications of channel subunits. The reduced inward calcium current densities (Fig. 7) would be expected to reduce calcium-induced calcium release from intracellular calcium stores, potentially contributing to the reductions in calcium transient amplitudes (Fig. 6 A).

Based on our observation that molecular hypercontractility drives downstream changes in cellular calcium handling and electrophysiology, we propose that mutation-induced changes in cellular tension alter mechanosensitive signaling pathways in cardiomyocytes (Saucerman et al., 2019). Consistent with this idea, we recently demonstrated that a dilated cardiomyopathy mutation in troponin T, ΔK210, affects molecular tension and mechanosensing, which helps to drive the disease progression (Clippinger et al., 2019). Similarly, increases in cardiac tension from external sources, including hypertensive disease and aortic stenosis, promote pathological hypertrophy. Deciphering the mechanobiological pathways in cardiomyocytes is an active field of research (Prosser et al., 2011; Robison et al., 2016; Saucerman et al., 2019). Hypercontractility of cardiomyocytes can impose aberrant stretch on fibroblasts, activating the transition to myofibroblasts (Saucerman et al., 2019) and contributing to the diffuse myocardial fibrosis frequently seen with HCM.

Implications for modeling and treating HCM

Modeling HCM is challenging since it is a complex disease where different adaptive and maladaptive pathways are activated as the disease progresses. Our goal was to connect the initial molecular insult with the early disease pathogenesis in human cells. We therefore used genome-edited hiPSC-CMs, which are excellent tools for dissecting the early disease pathogenesis (Lam and Wu, 2018). These experiments used isogenic cells, making it easier to decipher the direct consequences of the mutation on a controlled genetic background. R92Q hiPSC-CMs recapitulate some important aspects of HCM-induced changes in contractility (Tardiff et al., 1999; Robinson et al., 2002; Ford et al., 2012), altered electrophysiology (Coppini et al., 2017; Robinson et al., 2018), and calcium dysfunction (Rice et al., 2010; Ferrantini et al., 2017; Robinson et al., 2018) seen in other model systems. It should be noted that hPSC-CMs have several important limitations (see limitations section below). Limitations aside, hiPSC-CMs are powerful tools for studying the connection between the initial molecular insult and the early disease pathogenesis in human cells.

Our identification of altered cellular mechanics and downstream mechanobiological signaling pathways as key drivers of the disease has important implications for therapeutics. There is currently an outstanding need to develop new strategies to treat HCM. Our results suggest that targeting mechanobiological signaling pathways in cardiomyocytes could be useful for treating some forms of HCM.

We believe that cardiomyopathies are excellent candidates for a precision medicine approach (McNally and Mestroni, 2017; Fatkin et al., 2019; Lavine and Greenberg, 2020; Greenberg and Tardiff, 2021). Recently, there was a report of a HCM mutation in α-actinin linked to action potential prolongation attributed to increased calcium current density (Prondzynski et al., 2019), and the patient harboring this mutation was successfully treated with the L-type calcium channel blocker diltiazem. In R92Q, we observed a reduction in the calcium current density (Fig. 7), and therefore, a different therapeutic strategy would be necessary. Similarly, hiPSC-CMs harboring an HCM-linked mutation in troponin T, I79N, display changes in the action potential durations due to altered sodium–calcium exchanger function. Again, the cellular mechanism is distinct from that observed for R92Q, which is associated with changes in the inward calcium current density, potentially suggesting different therapeutic strategies (Wang et al., 2017; Wang et al., 2018). The marked differences between the functional effects of different HCM mutations highlight the need to understand the underlying derangements in molecular and cellular function when designing therapies.

Limitations

In our molecular studies, we were interested in uncovering the initial molecular insult of the R92Q mutation in troponin T that drives the early disease pathogenesis. As such, we focused on the

Downloaded from http://rupress.org/jgp/article-pdf/153/5/e202012787/1413510/jgp_202012787.pdf by Washington University In St. Louis Libraries user on 01 May 2021

effects of the mutation on calcium-dependent thin filament activation. Our experiments and computational modeling used well-established methods (McKillop and Geeves, 1993; Campbell et al., 2010) that are tailored to capture the effects of changes in thin filament function. It is important to note that other models exist that incorporate higher-order sarcomeric structures beyond the thin filament, including thick filament–based regulation of contractility (e.g., the super-relaxed state of myosin in the thick filament that modulates the number of available cross-bridges, mutation-induced alterations in the force per cross-bridge, and myosin binding protein C's role in thin filament activation). However, the potential impacts of the mutation on thick filament function, if present, are downstream of the initial molecular insult. That said, to a first-order approximation, our proposed molecular mechanism of mutation-induced changes in tropomyosin positioning is sufficient to explain the observed change in the calcium sensitivity of thin filament activation that we and others have observed.

Moreover, while our R92Q hiPSC-CMs recapitulate aspects of the early disease pathogenesis, they cannot fully capture the clinical phenotype for several reasons. First, hiPSC-CMs are developmentally immature, and they lack many of the physiological cues present in the myocardium (Lam and Wu, 2018; Musunuru et al., 2018). This immaturity includes expression of fetal genes (Fig. S4), spontaneous beating (Fig. 6), less negative resting membrane potentials (Fig. 7), and metabolic differences. As such, they do not capture aspects of clinical HCM, including fibrosis, myocyte disarray, and ventricular arrhythmias. While we employ several techniques to promote hiPSC-CM maturation, including plating the cells on physiological stiffness hydrogels, providing rectangular patterns to promote sarcomeric alignment, and aging cells at least 30 d before using them, these cells are still immature compared with adult cardiomyocytes (Ribeiro et al., 2015). Moreover, while patients are typically heterozygous for R92Q, our studies used homozygous cell lines to facilitate connecting the molecular and cellular phenotypes. It will be interesting to see how heterozygous cells differ from the homozygous cells used here. Despite these limitations, our gene-edited hPSC-CMs captured several aspects of the disease phenotype and enabled us to decipher the initial molecular insult from the activation of downstream adaptive and maladaptive signaling pathways.

Conclusions

We demonstrate that the initial insult of the R92Q mutation in troponin T is molecular hypercontractility at physiologically relevant calcium concentrations, which leads to alterations in mechanobiological signaling pathways that regulate calcium homeostasis, gene expression, and cellular electrophysiology. Taken together, our results demonstrate that mechanobiological adaptations are important in the early disease pathogenesis, and they suggest that targeting these pathways could open new avenues for treating HCM.

Acknowledgments

Olaf S. Andersen served as editor.

The authors thank Jonathan Davis for the troponin C^{T53C} plasmid.

This work was supported by the National Institutes of Health (grant R01 HL141086 to M.J. Greenberg and grants R01 HL034161 and R01 HL142520 to J.M. Nerbonne), the March of Dimes Foundation (grant FY18-BOC-430198 to M.J. Greenberg), the Children's Discovery Institute of Washington University and St. Louis Children's Hospital (grant PM-LI-2019-829 to M.J. Greenberg), the Washington University Institute of Materials Science, and the Washington University Center for Cellular Imaging (grant CDI-CORE-2015-505 to M.J. Greenberg). S.R. Clippinger was supported through a National Institutes of Health institutional training grant (T32 EB018266).

The authors declare no competing financial interests.

Author contributions: S.R. Clippinger purified proteins and performed and analyzed the stopped-flow and fluorescence experiments. P.E. Cloonan performed and analyzed the traction force microscopy experiments with the stem cell–derived cardiomyocytes. W. Wang performed and analyzed electrophysiological experiments. L. Greenberg purified proteins, implemented the cell-based assays, performed and analyzed experiments with stem cell–derived cardiomyocytes, performed RT-qPCR measurements, and performed calcium imaging experiments. W.T. Stump designed tools for microcontact printing. P. Angsutararux performed in vitro motility assays. J.M. Nerbonne oversaw the electrophysiological experiments and analyzed data. M.J. Greenberg oversaw the project, performed simulations, generated mutant proteins, implemented biochemical assays, analyzed data, and drafted the manuscript. All authors contributed to the writing and/or editing of the manuscript.

Submitted: 5 October 2020
Accepted: 18 March 2021

References

Adhikari, A.S., D.V. Trivedi, S.S. Sarkar, D. Song, K.B. Kooiker, D. Bernstein, J.A. Spudich, and K.M. Ruppel. 2019. β-Cardiac myosin hypertrophic cardiomyopathy mutations release sequestered heads and increase enzymatic activity. *Nat. Commun.* 10:2685. https://doi.org/10.1038/s41467-019-10555-9

Alamo, L., J.S. Ware, A. Pinto, R.E. Gillilan, J.G. Seidman, C.E. Seidman, and R. Padrón. 2017. Effects of myosin variants on interacting-heads motif explain distinct hypertrophic and dilated cardiomyopathy phenotypes. *eLife.* 6:e24634. https://doi.org/10.7554/eLife.24634

Barrick, S.K., S.R. Clippinger, L. Greenberg, and M.J. Greenberg. 2019. Computational tool to study perturbations in muscle regulation and its application to heart disease. *Biophys. J.* 116:2246–2252. https://doi.org/10.1016/j.bpj.2019.05.002

Bers, D.M. 2002. Cardiac excitation-contraction coupling. *Nature.* 415:198–205. https://doi.org/10.1038/415198a

Bers, D.M., C.W. Patton, and R. Nuccitelli. 2010. A practical guide to the preparation of Ca^{2+} buffers. *Methods Cell Biol.* 99:1–26. https://doi.org/10.1016/B978-0-12-374841-6.00001-3

Cai, W., J. Zhang, W.J. de Lange, Z.R. Gregorich, H. Karp, E.T. Farrell, S.D. Mitchell, T. Tucholski, Z. Lin, M. Biermann, et al. 2019. An unbiased proteomics method to assess the maturation of human pluripotent stem cell-derived cardiomyocytes. *Circ. Res.* 125:936–953. https://doi.org/10.1161/CIRCRESAHA.119.315305

Campbell, S.G., F.V. Lionetti, K.S. Campbell, and A.D. McCulloch. 2010. Coupling of adjacent tropomyosins enhances cross-bridge-mediated cooperative activation in a markov model of the cardiac thin filament. *Biophys. J.* 98:2254–2264. https://doi.org/10.1016/j.bpj.2010.02.010

Chandra, M., V.L. Rundell, J.C. Tardiff, L.A. Leinwand, P.P. De Tombe, and R.J. Solaro. 2001. Ca(2+) activation of myofilaments from transgenic mouse hearts expressing R92Q mutant cardiac troponin T. *Am. J. Physiol. Heart*

Downloaded from http://rupress.org/jgp/article-pdf/153/5/e202012787/1413510/jgp_202012787.pdf by Washington University In St. Louis Libraries user on 01 May 2021

Circ. Physiol. 280:H705–H713. https://doi.org/10.1152/ajpheart.2001.280.2.H705

Chowdhury, S.A.K., C.M. Warren, J.N. Simon, D.M. Ryba, A. Batra, P. Varga, E.G. Kranias, J.C. Tardiff, R.J. Solaro, and B.M. Wolska. 2020. Modifications of sarcoplasmic reticulum function prevent progression of sarcomere-linked hypertrophic cardiomyopathy despite a persistent increase in myofilament calcium response. *Front. Physiol.* 11:107. https://doi.org/10.3389/fphys.2020.00107

Clippinger, S.R., P.E. Cloonan, L. Greenberg, M. Ernst, W.T. Stump, and M.J. Greenberg. 2019. Disrupted mechanobiology links the molecular and cellular phenotypes in familial dilated cardiomyopathy. *Proc. Natl. Acad. Sci. USA.* 116:17831–17840. https://doi.org/10.1073/pnas.1910962116

Coppini, R., L. Mazzoni, C. Ferrantini, F. Gentile, J.M. Pioner, A. Laurino, L. Santini, V. Bargelli, M. Rotellini, G. Bartolucci, et al. 2017. Ranolazine prevents phenotype development in a mouse model of hypertrophic cardiomyopathy. *Circ. Heart Fail.* 10. e003565. https://doi.org/10.1161/CIRCHEARTFAILURE.116.003565

Davis, J.P., C. Norman, T. Kobayashi, R.J. Solaro, D.R. Swartz, and S.B. Tikunova. 2007. Effects of thin and thick filament proteins on calcium binding and exchange with cardiac troponin C. *Biophys. J.* 92:3195–3206. https://doi.org/10.1529/biophysj.106.095406

Davis, J., L.C. Davis, R.N. Correll, C.A. Makarewich, J.A. Schwanekamp, F. Moussavi-Harami, D. Wang, A.J. York, H. Wu, S.R. Houser, et al. 2016. A tension-based model distinguishes hypertrophic versus dilated cardiomyopathy. *Cell.* 165:1147–1159. https://doi.org/10.1016/j.cell.2016.04.002

Deacon, J.C., M.J. Bloemink, H. Rezavandi, M.A. Geeves, and L.A. Leinwand. 2012. Identification of functional differences between recombinant human α and β cardiac myosin motors. *Cell. Mol. Life Sci.* 69:2261–2277. https://doi.org/10.1007/s00018-012-0927-3

Debold, E.P., J.P. Schmitt, J.B. Patlak, S.E. Beck, J.R. Moore, J.G. Seidman, C. Seidman, and D.M. Warshaw. 2007. Hypertrophic and dilated cardiomyopathy mutations differentially affect the molecular force generation of mouse alpha-cardiac myosin in the laser trap assay. *Am. J. Physiol. Heart Circ. Physiol.* 293:H284–H291. https://doi.org/10.1152/ajpheart.00128.2007

Efron, B. 1979. Bootstrap Methods: Another Look at the Jackknife. *Ann. Stat.* 7:1–26. https://doi.org/10.1214/aos/1176344552

Fatkin, D., I.G. Huttner, J.C. Kovacic, J.G. Seidman, and C.E. Seidman. 2019. Precision medicine in the management of dilated cardiomyopathy: JACC State-of-the-Art Review. *J. Am. Coll. Cardiol.* 74:2921–2938. https://doi.org/10.1016/j.jacc.2019.10.011

Ferrantini, C., R. Coppini, J.M. Pioner, F. Gentile, B. Tosi, L. Mazzoni, B. Scellini, N. Piroddi, A. Laurino, L. Santini, et al. 2017. Pathogenesis of hypertrophic cardiomyopathy is mutation rather than disease specific: A comparison of the cardiac troponin T E163R and R92Q mouse models. *J. Am. Heart Assoc.* 6. e005407. https://doi.org/10.1161/JAHA.116.005407

Ford, S.J., R. Mamidi, J. Jimenez, J.C. Tardiff, and M. Chandra. 2012. Effects of R92 mutations in mouse cardiac troponin T are influenced by changes in myosin heavy chain isoform. *J. Mol. Cell. Cardiol.* 53:542–551. https://doi.org/10.1016/j.yjmcc.2012.07.018

Gangadharan, B., M.S. Sunitha, S. Mukherjee, R.R. Chowdhury, F. Haque, N. Sekar, R. Sowdhamini, J.A. Spudich, and J.A. Mercer. 2017. Molecular mechanisms and structural features of cardiomyopathy-causing troponin T mutants in the tropomyosin overlap region. *Proc. Natl. Acad. Sci. USA.* 114:11115–11120. https://doi.org/10.1073/pnas.1710354114

Greenberg, M.J., and J.C. Tardiff. 2021. Complexity in genetic cardiomyopathies and new approaches for mechanism-based precision medicine. *J. Gen. Physiol.* 153:e202012662. https://doi.org/10.1085/jgp.202012662

Greenberg, M.J., K. Kazmierczak, D. Szczesna-Cordary, and J.R. Moore. 2010. Cardiomyopathy-linked myosin regulatory light chain mutations disrupt myosin strain-dependent biochemistry. *Proc. Natl. Acad. Sci. USA.* 107:17403–17408. https://doi.org/10.1073/pnas.1009619107

Greenberg, M.J., H. Shuman, and E.M. Ostap. 2014. Inherent force-dependent properties of β-cardiac myosin contribute to the force-velocity relationship of cardiac muscle. *Biophys. J.* 107:L41–L44. https://doi.org/10.1016/j.bpj.2014.11.005

Harvey, P.A., and L.A. Leinwand. 2011. Cellular mechanisms of cardiomyopathy. *J. Cell Biol.* 194:355–365. https://doi.org/10.1083/jcb.201101100

Jinek, M., K. Chylinski, I. Fonfara, M. Hauer, J.A. Doudna, and E. Charpentier. 2012. A programmable dual-RNA-guided DNA endonuclease in adaptive bacterial immunity. *Science.* 337:816–821. https://doi.org/10.1126/science.1225829

Johnson, D., L. Zhu, M. Landim-Vieira, J.R. Pinto, and J.M. Chalovich. 2019. Basic residues within the cardiac troponin T C terminus are required for full inhibition of muscle contraction and limit activation by calcium. *J. Biol. Chem.* 294:19535–19545. https://doi.org/10.1074/jbc.RA119.010966

Lam, C.K., and J.C. Wu. 2018. Disease modelling and drug discovery for hypertrophic cardiomyopathy using pluripotent stem cells: how far have we come? *Eur. Heart J.* 39:3893–3895. https://doi.org/10.1093/eurheartj/ehy388

Lavine, K.J., and M.J. Greenberg. 2020. Beyond genomics-technological advances improving the molecular characterization and precision treatment of heart failure. *Heart Fail. Rev.* 26:405–415. https://doi.org/10.1007/s10741-020-10021-5

Lehman, W., R. Craig, and P. Vibert. 1994. Ca^{2+}-induced tropomyosin movement in Limulus thin filaments revealed by three-dimensional reconstruction. *Nature.* 368:65–67. https://doi.org/10.1038/368065a0

Lian, X., C. Hsiao, G. Wilson, K. Zhu, L.B. Hazeltine, S.M. Azarin, K.K. Raval, J. Zhang, T.J. Kamp, and S.P. Palecek. 2012. Robust cardiomyocyte differentiation from human pluripotent stem cells via temporal modulation of canonical Wnt signaling. *Proc. Natl. Acad. Sci. USA.* 109:E1848–E1857. https://doi.org/10.1073/pnas.1200250109

Lian, X., J. Zhang, S.M. Azarin, K. Zhu, L.B. Hazeltine, X. Bao, C. Hsiao, T.J. Kamp, and S.P. Palecek. 2013. Directed cardiomyocyte differentiation from human pluripotent stem cells by modulating Wnt/β-catenin signaling under fully defined conditions. *Nat. Protoc.* 8:162–175. https://doi.org/10.1038/nprot.2012.150

Liu, B., S.B. Tikunova, K.P. Kline, J.K. Siddiqui, and J.P. Davis. 2012. Disease-related cardiac troponins alter thin filament Ca2+ association and dissociation rates. *PLoS One.* 7:e38259. https://doi.org/10.1371/journal.pone.0038259

Livak, K.J., and T.D. Schmittgen. 2001. Analysis of relative gene expression data using real-time quantitative PCR and the $2^{-\Delta\Delta C(T)}$ method. *Methods.* 25:402–408. https://doi.org/10.1006/meth.2001.1262

Madan, A., M.C. Viswanathan, K.C. Woulfe, W. Schmidt, A. Sidor, T. Liu, T.H. Nguyen, B. Trinh, C. Wilson, S. Madathil, et al. 2020. *TNNT2* mutations in the tropomyosin binding region of TNT1 disrupt its role in contractile inhibition and stimulate cardiac dysfunction. *Proc. Natl. Acad. Sci. USA.* 117:18822–18831. https://doi.org/10.1073/pnas.2001692117

Malmqvist, U.P., A. Aronshtam, and S. Lowey. 2004. Cardiac myosin isoforms from different species have unique enzymatic and mechanical properties. *Biochemistry.* 43:15058–15065. https://doi.org/10.1021/bi0495329

Manning, E.P., J.C. Tardiff, and S.D. Schwartz. 2011. A model of calcium activation of the cardiac thin filament. *Biochemistry.* 50:7405–7413. https://doi.org/10.1021/bi200506k

Marian, A.J., G. Zhao, Y. Seta, R. Roberts, and Q.T. Yu. 1997. Expression of a mutant (Arg92Gln) human cardiac troponin T, known to cause hypertrophic cardiomyopathy, impairs adult cardiac myocyte contractility. *Circ. Res.* 81:76–85. https://doi.org/10.1161/01.RES.81.1.76

Martin, M.A. 2007. Bootstrap hypothesis testing for some common statistical problems: A critical evaluation of size and power properties. *Comput. Stat. Data Anal.* 51:6321–6342. https://doi.org/10.1016/j.csda.2007.01.020

McConnell, M., L. Tal Grinspan, M.R. Williams, M.L. Lynn, B.A. Schwartz, O.Z. Fass, S.D. Schwartz, and J.C. Tardiff. 2017. Clinically divergent mutation effects on the structure and function of the human cardiac tropomyosin overlap. *Biochemistry.* 56:3403–3413. https://doi.org/10.1021/acs.biochem.7b00266

McKillop, D.F., and M.A. Geeves. 1993. Regulation of the interaction between actin and myosin subfragment 1: evidence for three states of the thin filament. *Biophys. J.* 65:693–701. https://doi.org/10.1016/S0006-3495(93)81110-X

McNally, E.M., and L. Mestroni. 2017. Dilated cardiomyopathy: Genetic determinants and mechanisms. *Circ. Res.* 121:731–748. https://doi.org/10.1161/CIRCRESAHA.116.309396

McNamara, J.W., A. Li, N.J. Smith, S. Lal, R.M. Graham, K.B. Kooiker, S.J. van Dijk, C.G.D. Remedios, S.P. Harris, and R. Cooke. 2016. Ablation of cardiac myosin binding protein-C disrupts the super-relaxed state of myosin in murine cardiomyocytes. *J. Mol. Cell. Cardiol.* 94:65–71. https://doi.org/10.1016/j.yjmcc.2016.03.009

Morimoto, S., F. Yanaga, R. Minakami, and I. Ohtsuki. 1998. Ca2+-sensitizing effects of the mutations at Ile-79 and Arg-92 of troponin T in hypertrophic cardiomyopathy. *Am. J. Physiol.* 275:C200–C207. https://doi.org/10.1152/ajpcell.1998.275.1.C200

Mun, J.Y., M.J. Previs, H.Y. Yu, J. Gulick, L.S. Tobacman, S. Beck Previs, J. Robbins, D.M. Warshaw, and R. Craig. 2014. Myosin-binding protein C displaces tropomyosin to activate cardiac thin filaments and governs their speed by an independent mechanism. *Proc. Natl. Acad. Sci. USA.* 111:2170–2175. https://doi.org/10.1073/pnas.1316001111

Downloaded from http://rupress.org/jgp/article-pdf/153/5/e202012787/1413510/jgp_202012787.pdf by Washington University In St. Louis Libraries user on 01 May 2021

Musunuru, K., F. Sheikh, R.M. Gupta, S.R. Houser, K.O. Maher, D.J. Milan, A. Terzic, and J.C. Wu; American Heart Association Council on Functional Genomics and Translational Biology; Council on Cardiovascular Disease in the Young; and Council on Cardiovascular and Stroke Nursing. 2018. Induced pluripotent stem cells for cardiovascular disease modeling and precision medicine: A scientific statement from the American Heart Association. *Circ. Genom. Precis. Med.* 11. e000043. https://doi.org/10.1161/HCG.0000000000000043

Nag, S., D.V. Trivedi, S.S. Sarkar, A.S. Adhikari, M.S. Sunitha, S. Sutton, K.M. Ruppel, and J.A. Spudich. 2017. The myosin mesa and the basis of hypercontractility caused by hypertrophic cardiomyopathy mutations. *Nat. Struct. Mol. Biol.* 24:525–533. https://doi.org/10.1038/nsmb.3408

Napierski, N.C., K. Granger, P.R. Langlais, H.R. Moran, J. Strom, K. Touma, and S.P. Harris. 2020. A novel "cut and paste" method for in situ replacement of cMyBP-C reveals a new role for cMyBP-C in the regulation of contractile oscillations. *Circ. Res.* 126:737–749. https://doi.org/10.1161/CIRCRESAHA.119.315760

Press, W.H. 1992. Numerical recipes in C: the art of scientific computing. Second edition. Cambridge University Press, Cambridge, New York. 994 pp.

Prondzynski, M., M.D. Lemoine, A.T. Zech, A. Horváth, V. Di Mauro, J.T. Koivumäki, N. Kresin, J. Busch, T. Krause, E. Krämer, et al. 2019. Disease modeling of a mutation in α-actinin 2 guides clinical therapy in hypertrophic cardiomyopathy. *EMBO Mol. Med.* 11:e11115. https://doi.org/10.15252/emmm.201911115

Prosser, B.L., C.W. Ward, and W.J. Lederer. 2011. X-ROS signaling: rapid mechano-chemo transduction in heart. *Science.* 333:1440–1445. https://doi.org/10.1126/science.1202768

Ribeiro, A.J.S., O. Schwab, M.A. Mandegar, Y.S. Ang, B.R. Conklin, D. Srivastava, and B.L. Pruitt. 2017. Multi-imaging method to assay the contractile mechanical output of micropatterned fuman iPSC-derived cardiac myocytes. *Circ. Res.* 120:1572–1583. https://doi.org/10.1161/CIRCRESAHA.116.310363

Ribeiro, A.J., Y.S. Ang, J.D. Fu, R.N. Rivas, T.M. Mohamed, G.C. Higgs, D. Srivastava, and B.L. Pruitt. 2015. Contractility of single cardiomyocytes differentiated from pluripotent stem cells depends on physiological shape and substrate stiffness. *Proc. Natl. Acad. Sci. USA.* 112:12705–12710. https://doi.org/10.1073/pnas.1508073112

Rice, R., P. Guinto, C. Dowell-Martino, H. He, K. Hoyer, M. Krenz, J. Robbins, J.S. Ingwall, and J.C. Tardiff. 2010. Cardiac myosin heavy chain isoform exchange alters the phenotype of cTnT-related cardiomyopathies in mouse hearts. *J. Mol. Cell. Cardiol.* 48:979–988. https://doi.org/10.1016/j.yjmcc.2009.11.018

Risi, C., B. Belknap, E. Forgacs-Lonart, S.P. Harris, G.F. Schröder, H.D. White, and V.E. Galkin. 2018. N-terminal domains of cardiac myosin binding protein C cooperatively activate the thin filament. *Structure.* 26:1604–1611.e4. https://doi.org/10.1016/j.str.2018.08.007

Robinson, P., M. Mirza, A. Knott, H. Abdulrazzak, R. Willott, S. Marston, H. Watkins, and C. Redwood. 2002. Alterations in thin filament regulation induced by a human cardiac troponin T mutant that causes dilated cardiomyopathy are distinct from those induced by troponin T mutants that cause hypertrophic cardiomyopathy. *J. Biol. Chem.* 277:40710–40716. https://doi.org/10.1074/jbc.M203446200

Robinson, P., P.J. Griffiths, H. Watkins, and C.S. Redwood. 2007. Dilated and hypertrophic cardiomyopathy mutations in troponin and alpha-tropomyosin have opposing effects on the calcium affinity of cardiac thin filaments. *Circ. Res.* 101:1266–1273. https://doi.org/10.1161/CIRCRESAHA.107.156380

Robinson, P., X. Liu, A. Sparrow, S. Patel, Y.H. Zhang, B. Casadei, H. Watkins, and C. Redwood. 2018. Hypertrophic cardiomyopathy mutations increase myofilament Ca^{2+} buffering, alter intracellular Ca^{2+} handling, and stimulate Ca^{2+}-dependent signaling. *J. Biol. Chem.* 293:10487–10499. https://doi.org/10.1074/jbc.RA118.002081

Robison, P., M.A. Caporizzo, H. Ahmadzadeh, A.I. Bogush, C.Y. Chen, K.B. Margulies, V.B. Shenoy, and B.L. Prosser. 2016. Detyrosinated microtubules buckle and bear load in contracting cardiomyocytes. *Science.* 352:aaf0659. https://doi.org/10.1126/science.aaf0659

Rust, E.M., F.P. Albayya, and J.M. Metzger. 1999. Identification of a contractile deficit in adult cardiac myocytes expressing hypertrophic cardiomyopathy-associated mutant troponin T proteins. *J. Clin. Invest.* 103:1459–1467. https://doi.org/10.1172/JCI6377

Sato, Y., D.G. Ferguson, H. Sako, G.W. Dorn II, V.J. Kadambi, A. Yatani, B.D. Hoit, R.A. Walsh, and E.G. Kranias. 1998. Cardiac-specific overexpression of mouse cardiac calsequestrin is associated with depressed cardiovascular function and hypertrophy in transgenic mice. *J. Biol. Chem.* 273:28470–28477. https://doi.org/10.1074/jbc.273.43.28470

Saucerman, J.J., P.M. Tan, K.S. Buchholz, A.D. McCulloch, and J.H. Omens. 2019. Mechanical regulation of gene expression in cardiac myocytes and fibroblasts. *Nat. Rev. Cardiol.* 16:361–378. https://doi.org/10.1038/s41569-019-0155-8

Schindelin, J., I. Arganda-Carreras, E. Frise, V. Kaynig, M. Longair, T. Pietzsch, S. Preibisch, C. Rueden, S. Saalfeld, B. Schmid, et al. 2012. Fiji: an open-source platform for biological-image analysis. *Nat. Methods.* 9:676–682. https://doi.org/10.1038/nmeth.2019

Schober, T., S. Huke, R. Venkataraman, O. Gryshchenko, D. Kryshtal, H.S. Hwang, F.J. Baudenbacher, and B.C. Knollmann. 2012. Myofilament Ca sensitization increases cytosolic Ca binding affinity, alters intracellular Ca homeostasis, and causes pause-dependent Ca-triggered arrhythmia. *Circ. Res.* 111:170–179. https://doi.org/10.1161/CIRCRESAHA.112.270041

Sharma, A., G. Li, K. Rajarajan, R. Hamaguchi, P.W. Burridge, and S.M. Wu. 2015. Derivation of highly purified cardiomyocytes from human induced pluripotent stem cells using small molecule-modulated differentiation and subsequent glucose starvation. *J. Vis. Exp.* (97). https://doi.org/10.3791/52628

Sheng, J.J., and J.P. Jin. 2014. Gene regulation, alternative splicing, and posttranslational modification of troponin subunits in cardiac development and adaptation: a focused review. *Front. Physiol.* 5:165. https://doi.org/10.3389/fphys.2014.00165

Sitbon, Y.H., K. Kazmierczak, J. Liang, S. Yadav, M. Veerasammy, R.M. Kanashiro-Takeuchi, and D. Szczesna-Cordary. 2020. Ablation of the N terminus of cardiac essential light chain promotes the super-relaxed state of myosin and counteracts hypercontractility in hypertrophic cardiomyopathy mutant mice. *FEBS J.* 287:3989–4004. https://doi.org/10.1111/febs.15243

Spudich, J.A. 2015. The myosin mesa and a possible unifying hypothesis for the molecular basis of human hypertrophic cardiomyopathy. *Biochem. Soc. Trans.* 43:64–72. https://doi.org/10.1042/BST20140324

Sung, J., S. Nag, K.I. Mortensen, C.L. Vestergaard, S. Sutton, K. Ruppel, H. Flyvbjerg, and J.A. Spudich. 2015. Harmonic force spectroscopy measures load-dependent kinetics of individual human β-cardiac myosin molecules. *Nat. Commun.* 6:7931. https://doi.org/10.1038/ncomms8931

Sweeney, H.L., H.S. Feng, Z. Yang, and H. Watkins. 1998. Functional analyses of troponin T mutations that cause hypertrophic cardiomyopathy: insights into disease pathogenesis and troponin function. *Proc. Natl. Acad. Sci. USA.* 95:14406–14410. https://doi.org/10.1073/pnas.95.24.14406

Szczesna, D., R. Zhang, J. Zhao, M. Jones, G. Guzman, and J.D. Potter. 2000. Altered regulation of cardiac muscle contraction by troponin T mutations that cause familial hypertrophic cardiomyopathy. *J. Biol. Chem.* 275:624–630. https://doi.org/10.1074/jbc.275.1.624

Tardiff, J.C., T.E. Hewett, B.M. Palmer, C. Olsson, S.M. Factor, R.L. Moore, J. Robbins, and L.A. Leinwand. 1999. Cardiac troponin T mutations result in allele-specific phenotypes in a mouse model for hypertrophic cardiomyopathy. *J. Clin. Invest.* 104:469–481. https://doi.org/10.1172/JCI6067

Tikunova, S.B., J.A. Rall, and J.P. Davis. 2002. Effect of hydrophobic residue substitutions with glutamine on Ca(2+) binding and exchange with the N-domain of troponin C. *Biochemistry.* 41:6697–6705. https://doi.org/10.1021/bi011763h

Tobacman, L.S., M. Nihli, C. Butters, M. Heller, V. Hatch, R. Craig, W. Lehman, and E. Homsher. 2002. The troponin tail domain promotes a conformational state of the thin filament that suppresses myosin activity. *J. Biol. Chem.* 277:27636–27642. https://doi.org/10.1074/jbc.M201768200

VanBuren, P., D.E. Harris, N.R. Alpert, and D.M. Warshaw. 1995. Cardiac V1 and V3 myosins differ in their hydrolytic and mechanical activities in vitro. *Circ. Res.* 77:439–444. https://doi.org/10.1161/01.RES.77.2.439

Wang, L., D.O. Kryshtal, K. Kim, S. Parikh, A.G. Cadar, K.R. Bersell, H. He, J.R. Pinto, and B.C. Knollmann. 2017. Myofilament calcium-buffering dependent action potential triangulation in human-induced pluripotent stem cell model of hypertrophic cardiomyopathy. *J. Am. Coll. Cardiol.* 70:2600–2602. https://doi.org/10.1016/j.jacc.2017.09.033

Wang, L., K. Kim, S. Parikh, A.G. Cadar, K.R. Bersell, H. He, J.R. Pinto, D.O. Kryshtal, and B.C. Knollmann. 2018. Hypertrophic cardiomyopathy-linked mutation in troponin T causes myofibrillar disarray and pro-arrhythmic action potential changes in human iPSC cardiomyocytes. *J. Mol. Cell. Cardiol.* 114:320–327. https://doi.org/10.1016/j.yjmcc.2017.12.002

Watkins, H., W.J. McKenna, L. Thierfelder, H.J. Suk, R. Anan, A. O'Donoghue, P. Spirito, A. Matsumori, C.S. Moravec, J.G. Seidman, et al. 1995. Mutations in the genes for cardiac troponin T and alpha-tropomyosin in

Downloaded from http://rupress.org/jgp/article-pdf/153/5/e202012787/1413510/jgp_202012787.pdf by Washington University In St. Louis Libraries user on 01 May 2021

hypertrophic cardiomyopathy. *N. Engl. J. Med.* 332:1058–1065. https://doi.org/10.1056/NEJM199504203321603

Williams, M.R., S.J. Lehman, J.C. Tardiff, and S.D. Schwartz. 2016. Atomic resolution probe for allostery in the regulatory thin filament. *Proc. Natl. Acad. Sci. USA.* 113:3257–3262. https://doi.org/10.1073/pnas.1519541113

Yamada, Y., K. Namba, and T. Fujii. 2020. Cardiac muscle thin filament structures reveal calcium regulatory mechanism. *Nat. Commun.* 11:153. https://doi.org/10.1038/s41467-019-14008-1

Yanaga, F., S. Morimoto, and I. Ohtsuki. 1999. Ca^{2+} sensitization and potentiation of the maximum level of myofibrillar ATPase activity caused by mutations of troponin T found in familial hypertrophic cardiomyopathy. *J. Biol. Chem.* 274:8806–8812. https://doi.org/10.1074/jbc.274.13.8806

Zhang, T., L.S. Maier, N.D. Dalton, S. Miyamoto, J. Ross Jr., D.M. Bers, and J.H. Brown. 2003. The deltaC isoform of CaMKII is activated in cardiac hypertrophy and induces dilated cardiomyopathy and heart failure. *Circ. Res.* 92:912–919. https://doi.org/10.1161/01.RES.0000069686.31472.C5

Downloaded from http://rupress.org/jgp/article-pdf/153/5/e202012787/1413510/jgp_202012787.pdf by Washington University In St. Louis Libraries user on 01 May 2021

Supplemental material

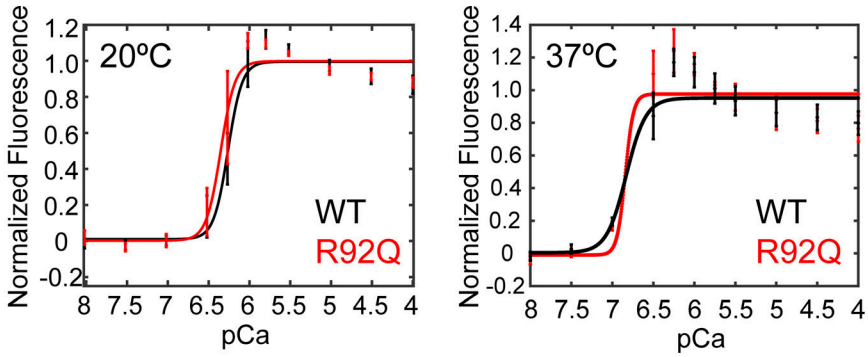

	WT (20°C)	R92Q (20°C)	p	WT (37°C)	R92Q (37°C)	p
IAANs Ca50 (μM) (n≥3)	0.55 (±0.10)	0.49 (±0.09)	0.36	0.14 (±0.11)	0.12(±0.07)	0.44
IAANs Hill (n≥3)	3.60 (±1.16)	6.59 (±2.20)	0.04	4.51 (±2.32)	8.94 (±4.33)	0.21

Figure S1. **Affinity of calcium binding to the troponin complex at 20°C and 37°C.** IAANS-labeled troponin C was reconstituted into regulated thin filaments. Titrations with increasing calcium were conducted. Error bars show the SD of greater than or equal to three experiments. Values derived from fits, standard errors in the fits, and P values are shown. P values were calculated using a two-tailed Student's *t* test.

Downloaded from http://rupress.org/jgp/article-pdf/153/5/e202012787/1413510/jgp_202012787.pdf by Washington University In St. Louis Libraries user on 01 May 2021

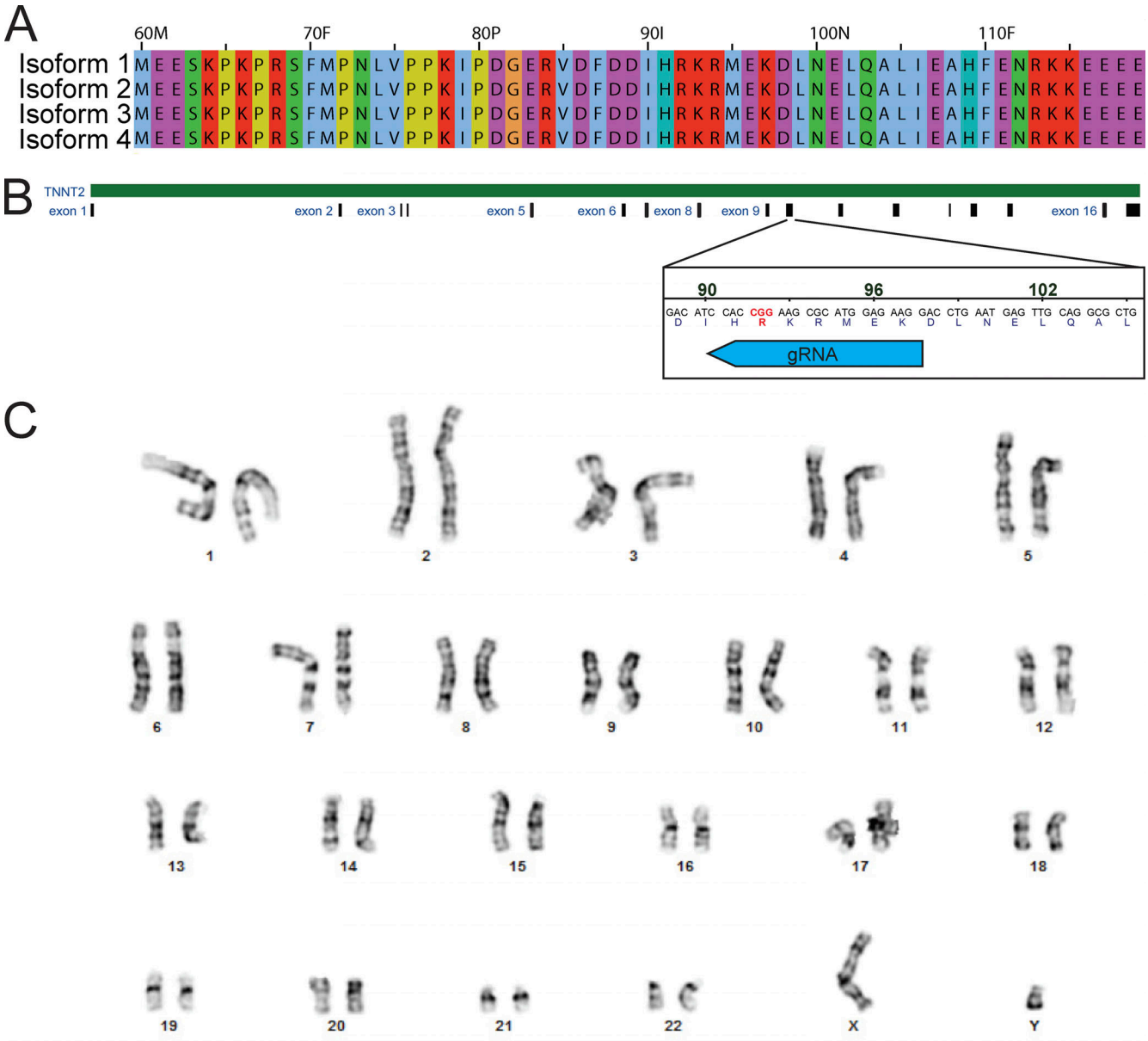

Figure S2. **Generation of gene-edited hiPSC-CMs. (A)** Sequence alignment of troponin T splice isoforms expressed in humans reveals that all isoforms contain the R92 residue. **(B)** CRISPR-Cas9 targeting of R92Q in troponin T. The R92Q mutation was added via homology-directed repair. The gRNA sequence for targeting was 5′-CCTTCTCCATGCGCTTCCGGNGG-3′. From our screen, 21% of the cells were homozygous for the R92Q mutation (CGG→CAA). **(C)** Karyotyping of R92Q gene-edited cells reveals a normal karyotype.

Downloaded from http://rupress.org/jgp/article-pdf/153/5/e202012787/1413510/jgp_202012787.pdf by Washington University In St. Louis Libraries user on 01 May 2021

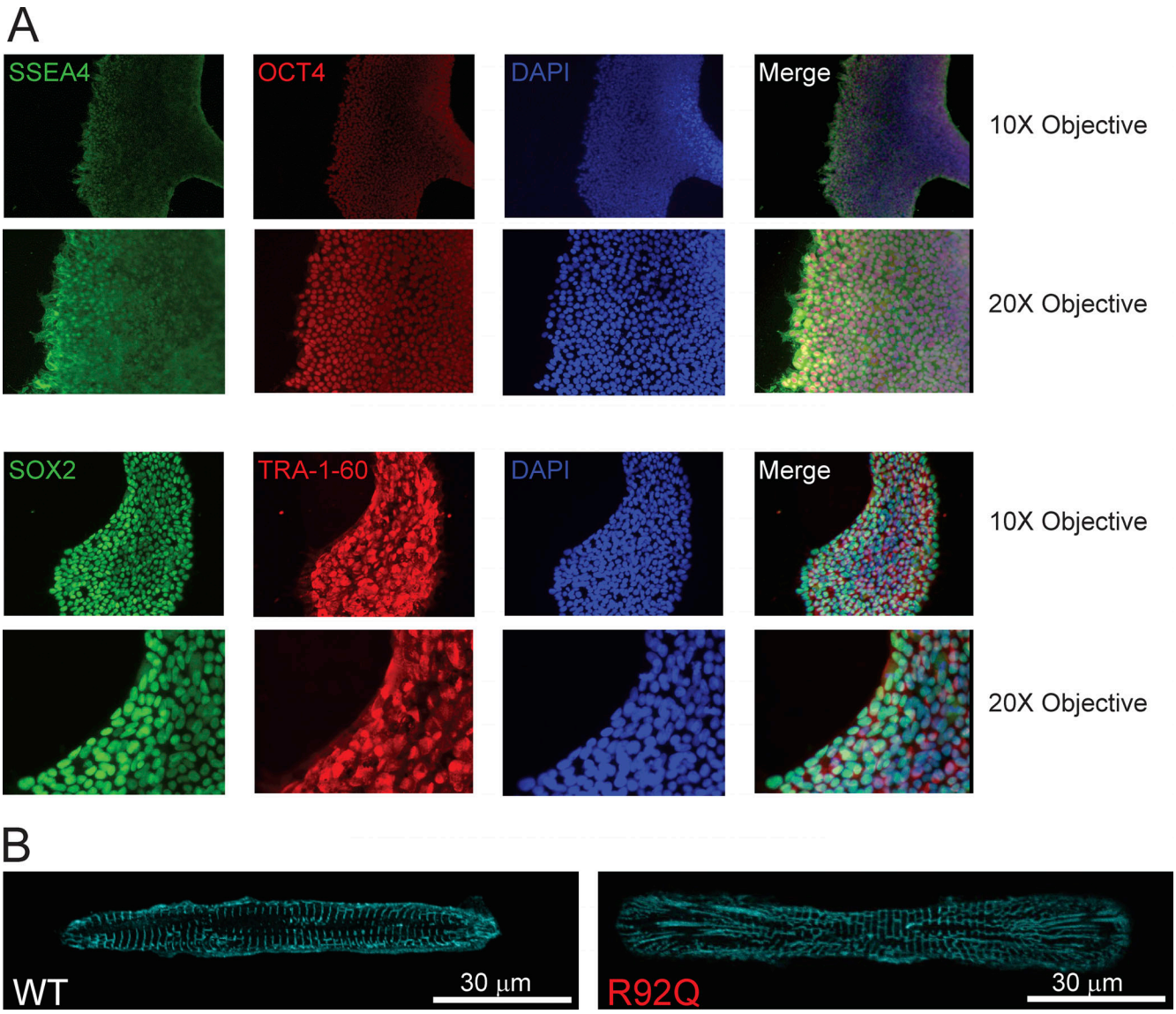

Figure S3. **Immunofluorescence images of stem cells and hiPSC-CMs. (A)** Pluripotency staining of R92Q cells. R92Q gene-edited cells are pluripotent as assessed by immunofluorescence staining for the markers SSEA4, OCT4, SOX2, and TRA-1-60. **(B)** Projections of hiPSC-CMs on glass stained for α-actinin to mark the sarcomeric Z-discs.

Downloaded from http://rupress.org/jgp/article-pdf/153/5/e202012787/1413510/jgp_202012787.pdf by Washington University In St. Louis Libraries user on 01 May 2021

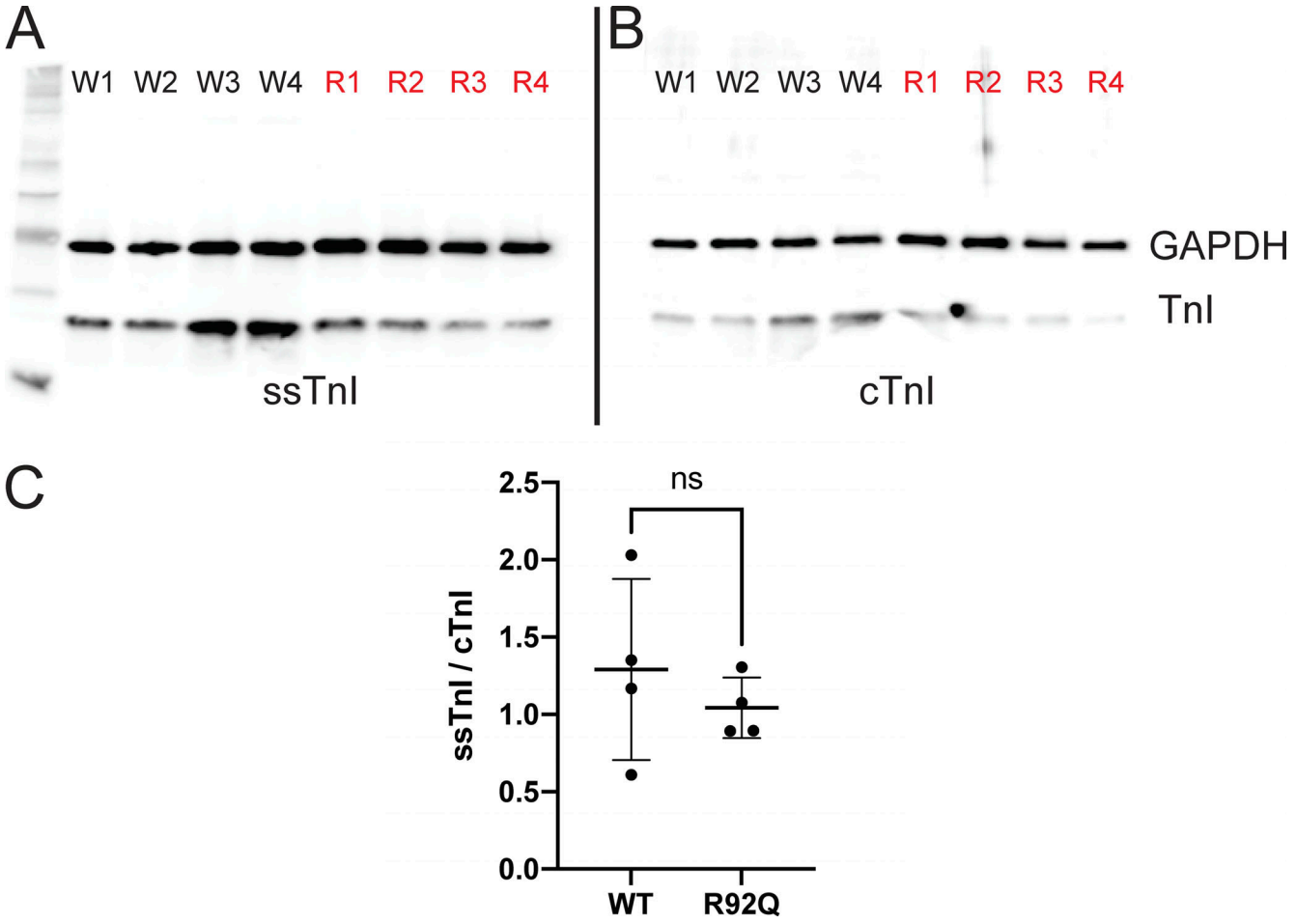

Figure S4. **Relative expression of fetal (slow skeletal) and adult (cardiac) troponin I isoforms in hiPSC-CMs. (A)** Western blot showing the expression of the fetal isoform of troponin I (slow skeletal troponin I [ssTnI]). Shown are four lysates from WT cells (W1, W2, W3, and W4) and four lysates from R92Q cells (R1, R2, R3, and R4). GAPDH is used as a loading control. **(B)** Western blot on a separate membrane showing the expression of the adult isoform of troponin I (cardiac troponin I [cTnI]). Shown are four lysates from WT cells (W1, W2, W3, and W4) and four lysates from R92Q cells (R1, R2, R3, and R4). GAPDH is used as a loading control. **(C)** Quantification of the ratio of ssTnI/cTnI was determined by densitometry. The TnI/GAPDH ratio was calculated for both ssTnI and cTnI and then divided to get the ratio. These is no difference in the ratio (ns, not significant [P = 0.49] by Mann–Whitney test).

Downloaded from http://rupress.org/jgp/article-pdf/153/5/e202012787/1413510/jgp_202012787.pdf by Washington University In St. Louis Libraries user on 01 May 2021

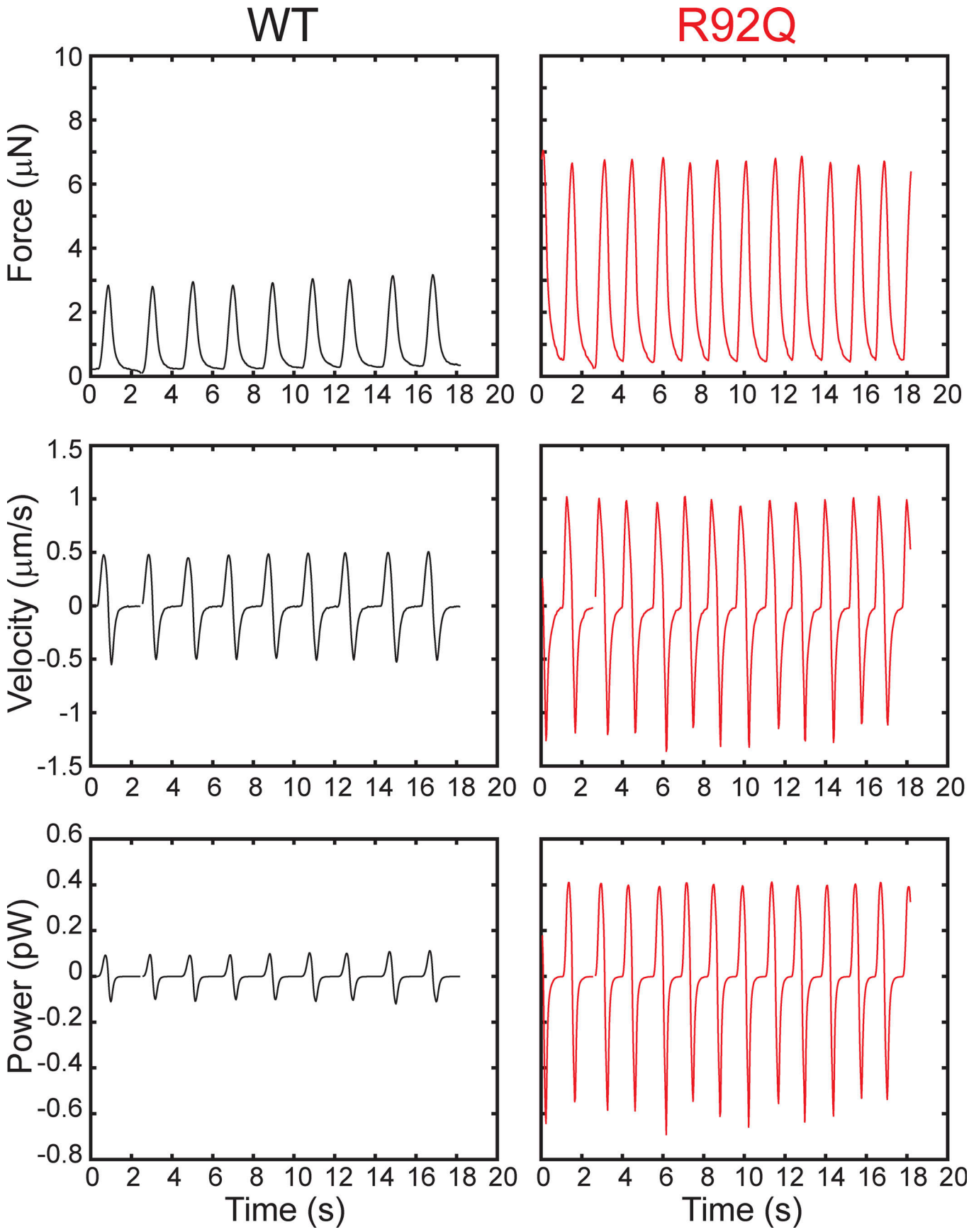

Figure S5. **Representative traces of hiPSC-CMs spontaneously beating on 10-kPa polyacrylamide gels measured by traction force microscopy.** Plotted are the force of contraction, the velocity, and the power output. Positive values denote shortening and negative values denote lengthening.

Downloaded from http://rupress.org/jgp/article-pdf/153/5/e202012787/1413510/jgp_202012787.pdf by Washington University In St. Louis Libraries user on 01 May 2021

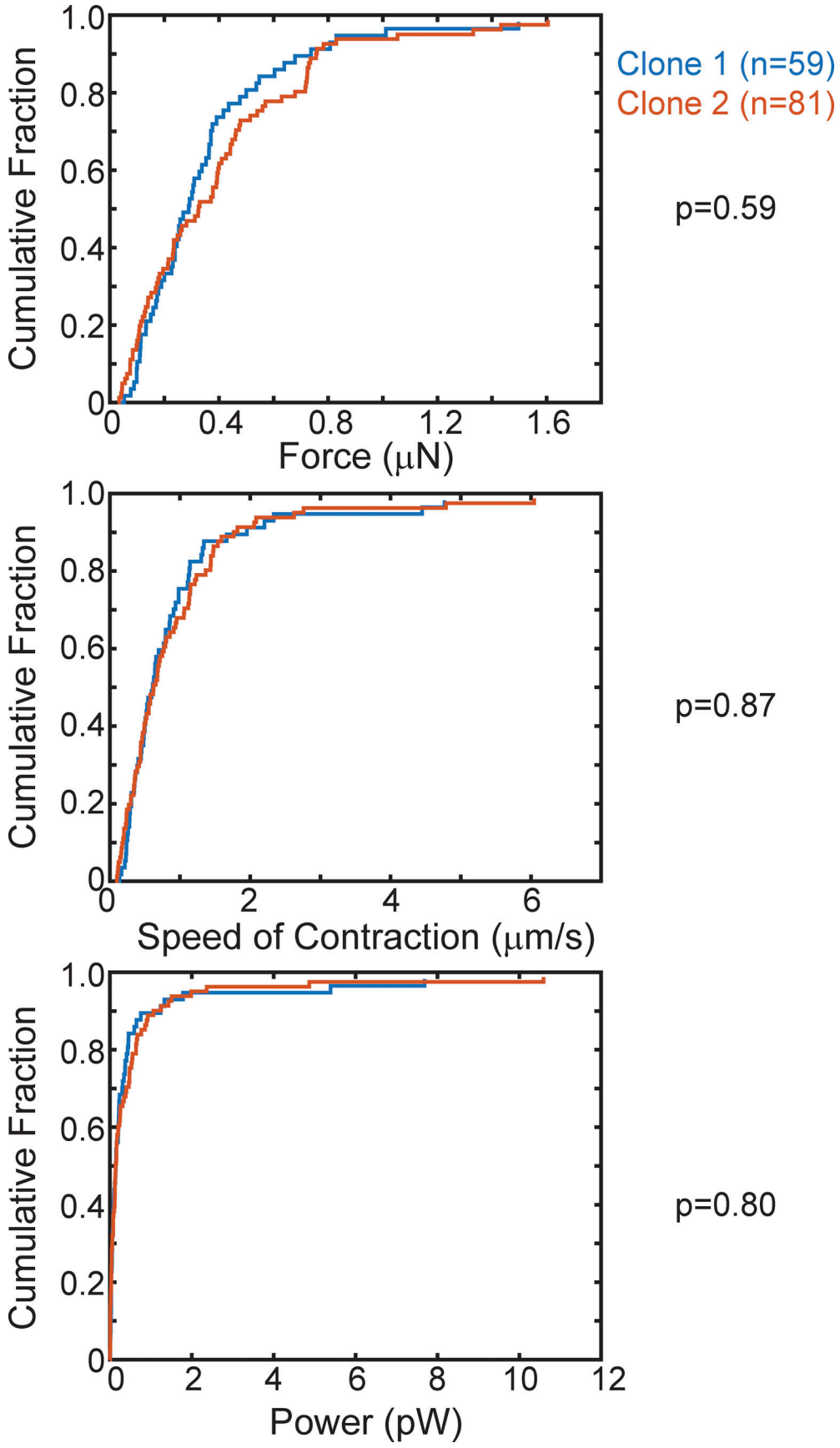

Figure S6. **Comparison of the two independently derived R92Q clones examined using traction force microscopy reveals no significant differences between the clones.** Cumulative distributions showing the force, speed, and power of contraction. P values are calculated from a Mann–Whitney *U* test.

Downloaded from http://rupress.org/jgp/article-pdf/153/5/e202012787/1413510/jgp_202012787.pdf by Washington University In St. Louis Libraries user on 01 May 2021

Video 1. **Displacement of beads by WT (gray) and R92Q (red) hiPSC-CMs contracting on a 10 kPa polyacrylamide gel.** Videos were recorded at 30 frames/s using a spinning disc confocal microscope (Nikon). The cell, which is not visible, is on a rectangular pattern of Matrigel with a 7:1 aspect ratio. The displacement of the beads was tracked as a function of time. Note that the two cells shown are not on the same slide/hydrogel; rather, we have merged two videos to facilitate direct visual comparison of the contractility in WT and mutant cells. As is evident in the video, force is generated primarily along the long axis of the cells. These videos were used to generate the representative traces in Fig. S5.

Three supplemental tables are provided online. Table S1 displays the RT-qPCR gene names and primers used in this study. Table S2 lists the RT-qPCR measurements of the expression of key calcium-handling genes. Table S3 provides the values from this study's electrophysiological experiments.

Downloaded from http://rupress.org/jgp/article-pdf/153/5/e202012787/1413510/jgp_202012787.pdf by Washington University In St. Louis Libraries user on 01 May 2021